Available online at www.sciencedirect.com

ScienceDirect

journal homepage: www.elsevier.com/locate/he

Hydrogen evolution and oxygen evolution reactions of pristine and alkali metal doped $SnSe_2$ monolayer

Archana N. Inamdar [a], *Narayan N. Som* [b], *Arun Pratap* [a], *Prafulla K. Jha* [b,*]

[a] *Department of Applied Physics, Faculty of Technology and Engineering, The Maharaja Sayajirao University of Baroda, Vadodara, 390001, India*

[b] *Department of Physics, Faculty of Science, The Maharaja Sayajirao University of Baroda, Vadodara, 390002, India*

HIGHLIGHTS

- The analysis of HER and OER activity is done for $SnSe_2$ and alkali atoms doped $SnSe_2$ monolayers.
- $SnSe_2$ having optical bandgap of 1.2 eV can be used as photo-electro catalyst.
- Basal plane activity of $SnSe_2$ is dopant dependent.
- Edge site of Na-doped $SnSe_2$ is best suited for hydrogen evolution reaction.
- Basal plane of Ca-doped $SnSe_2$ is best suited for oxygen evolution reaction.

GRAPHICAL ABSTRACT

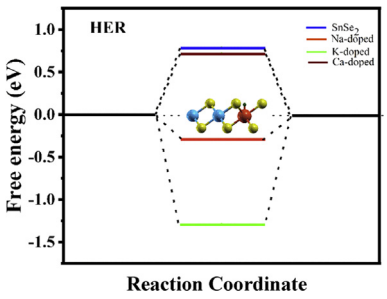

ARTICLE INFO

Article history:
Received 18 April 2019
Received in revised form
14 June 2019
Accepted 10 July 2019
Available online xxx

Keywords:
Metal di-selenides
Electrocatalyst
Density functional theory (DFT)
Hydrogen evolution reaction (HER)
Oxygen evolution reaction (OER)

ABSTRACT

Many transition metal di-selenides such as $MoSe_2$ and WSe_2 show good catalytic activity on their edges with limited active orientations. These metal di-selenides are actively being used as target material for increasing the number of electrocatalytic active sites and in turn to improve the hydrogen evolution reaction (HER) and oxygen evolution reaction (OER) activities by increasing the ratio of edges to the basal plane. In present work, we have studied the activity of pristine and alkali atoms (Na, K and Ca) doped-$SnSe_2$ for HER and OER catalyst. The *state-of-art* density functional theory (DFT) based computations are performed for estimating the catalytic activity of the pristine and doped $SnSe_2$ by means of evaluating the adsorption and Gibbs free energies subjected to hydrogen and oxygen adsorption. Further, to get better prediction of adsorption energy on the individual catalytic surface, we have included the dispersion correction term to exchange-correlation functional. Results show that the pristine $SnSe_2$ is not a good HER catalyst when hydrogen is adsorbed on its basal plane. However, edge-sites show the good hydrogen adsorption and

* *Corresponding author.*
E-mail addresses: prafullaj@yahoo.com, pk.jha-phy@msubaroda.ac.in (P.K. Jha).

https://doi.org/10.1016/j.ijhydene.2019.07.093

indicates that the edges of $SnSe_2$ are the most preferential site for hydrogen adsorption. As far as the catalytic activity of $SnSe_2$ with dopants is concerned, the Na-doped $SnSe_2$ among all shows the best catalytic activity over its edge-site; whereas K and Ca doped $SnSe_2$ show basal plane as preferred catalytic site. It is interesting to note that the disadvantage of low catalytic activity on basal plane of $SnSe_2$ can be improved by selective doping of alkali metals.

Introduction

The dilemma of global warming that is majorly caused by extensive utilization of fossil fuels [1], can be resolved by incorporating eco-friendly ways to harvest and/or generate green and clean energy. One of the cleanest way of energy production is to utilize hydrogen as a fuel that can be generated by breaking water molecules into its constituents, generalized as water-splitting. Further utilization of hydrogen is also done in the chemical industry for producing ammonia and methanol, and has many potential applications such as powering of vehicles, fuel cell, heating, aircraft and sulphur removal from the petroleum [2–4]. Among many methods to produce hydrogen, the electrochemical splitting of water (using photocatalyst/electrocatalyst/photoelectron catalyst) has gained significant attention due to its carbon free hydrogen generation [5–10]. The water-splitting procedure can be sub-divided into two half reactions: the evolution of H_2 that is represented by $2H^+ + 2e^- \rightarrow H_2$ and evolution of O_2 that is $2H_2O \rightarrow 4H^+ + 4e^- + O_2$. Difference in photocatalytic and electrocatalytic approaches for hydrogen evolution reaction (HER) is that the source generation carrier is generated via absorption of sunlight in the former case; whereas the latter one involves oxidation and reduction via direct electron transfer with lower potential chemical reactions. For a material to be utilized as an electrocatalyst, photocatalyst or electro-photocatalyst, certain criteria are to be satisfied. A good electrocatalyst reduces the overpotential of chemical reaction whereas a photocatalyst requires a moderate electronic band gap (1–2 eV) for optical photon absorption. For a material to be a photocatalyst and electro-photocatalyst respectively, the necessary conditions to be satisfied are,

$$E \geq E_g + E_a \text{ and } E \geq E_g + E_{AOP} \quad (1)$$

Where, E is the minimum energy required for splitting the water molecule, E_g is the band gap energy of semiconductor, E_a is the activation energy for a photocatalyst and E_{AOP} is the activation overpotential [6]. Up till now, many promising HER catalysts using non-noble transition metals, carbides, transition metal phosphides, pyrite type cobalt phosphide and nitrogen or boron doped graphene, arsenene with several dopants etc. have been predicted and developed [5–7,11–16]. However, the efficiency of production which is sensitive to the overpotential of the electrocatalyst has no alternative than the conventionally used expensive noble metals [5,17].

It is observed that the edges of metal chalcogenides act more reactively than their basal planes which is one of the hindrance for production of hydrogen [18]. To overcome this limitation, one needs to increase the ratio of edges to basal plane in these materials. $SnSe_2$ being from the group of metal chalcogenides can be assumed to have similar behaviour as MoS_2 and WS_2 and others belonging to the same group, which have recently gained special attention as a promising candidate for electrocatalyst due to its low cost fabrication and better electrocatalytic activity [5]. The density functional theory (DFT) report by Han et al. [19] based on generalized gradient approximation computations suggest that $SnSe_2$ monolayer exhibits semiconducting nature with band gap of 0.85 eV, indicating probable application of $SnSe_2$ as an electrocatalyst for hydrogen evolution reaction (HER). In addition, it is found that the introduction of doping induces metallic nature in $SnSe_2$ that further improves the HER activity at its basal plane [5,15]. This can also be attributed by the Density of States (DOS) value at Fermi level for all the three dopants i.e Na, K and Ca having values 5.394 States/eV, 5.986 States/eV and 7.047 States/eV respectively.

Tailoring of the electronic properties of material for enhancing its HER and/or OER activities can be done by applying external strain, electric field and doping [15,20,21]. A DFT based report shows that the HER catalytic activity of the $SnSe_{2(1-x)}S_{2x}$ monolayer on its basal plane gets enhanced after applying tensile strain [22]. Further reports on two dimensional materials like borophene [23], graphene [24] and graphitic nanosheet with metal borohydride nanodots [25] suggest that the hydrogen storage performance of these materials gets significantly improved after doping these materials with alkali-metals. The maximum capacity is reported for Li doped borophene [23].

In present work, we have examined the effect of doping (Na, K and Ca) on the HER and OER catalytic activities, work-function and optical properties of $SnSe_2$by utilizing first-principles dispersion corrected density functional theory based calculations. In addition, we have also investigated the interaction mechanism between hydrogen and oxygen gases with pristine and doped $SnSe_2$ for improvement of its electro catalytic activity.

Computational methodology

All computations in the present study were performed using *state-of-art* first-principles density functional theory (DFT) implemented within plane wave pseudopotential code Quantum Espresso [26]. The exchange correlation interaction

Please cite this article as: Inamdar AN et al., Hydrogen evolution and oxygen evolution reactions of pristine and alkali metal doped $SnSe_2$ monolayer, International Journal of Hydrogen Energy, https://doi.org/10.1016/j.ijhydene.2019.07.093

was treated within the generalised gradient approximation (GGA) given by Perdew-Burke-Ernzerhof (PBE) [27]. Further, the dispersion correction (D2) of Grimme has been employed throughout the calculation to get accurate value of adsorption energy for adsorbed hydrogen and oxygen adsorption. The kinetic energy and charge density cut-offs of 80 and 800 Ry respectively were sufficient to fully converge the lattice parameters and total energy within the specified threshold criterion. A slab of vacuum with 15 Å height was inserted above the monolayer to avoid the interaction between successive images. The reciprocal space was sampled by a dense grid of $9 \times 9 \times 1$ constructed under Monkhorst-Pack scheme [28]. The energy convergence value between two consecutive steps was chosen as 10^{-4} eV and convergence was repeated self-consistently until the maximum Hellmann-Feynman forces acting on each atom were less than 0.001 eV/Å. Furthermore, we have calculated optical absorption spectra of pristine and doped-$SnSe_2$ to examine the applicability of these systems to be utilized as a photo-electrocatalyst. The optical absorption spectra were calculated with the help of the frequency-dependent dielectric function. The real and imaginary parts of the dielectric function $\varepsilon(\omega) = \varepsilon_{real}(\omega) + \varepsilon_{imag}(\omega)$, can be obtained using Kramers-Kronig relation and defined as follows:

$$\alpha = \frac{2\sqrt{2}\pi e}{hc}\sqrt{\sqrt{\varepsilon_{real}^2(\omega) + \varepsilon_{imag}^2(\omega)} - \varepsilon_{real}(\omega)} \quad (2)$$

Results and discussion

Before computing the HER and OER catalytic activities of $SnSe_2$, we first individually optimised the pristine and alkali metal (Na, K and Ca) doped $SnSe_2$. Fig. 1(a) shows the well-optimised geometries of pristine $SnSe_2$, while Fig. 1(b) shows the same for alkali metal doped-$SnSe_2$. The $SnSe_2$ monolayer in its ground state possesses 2H phase. The 2H phase of $SnSe_2$ that has space group of P3 $m1$ contains octahedral coordination of the Sn atom surrounded by Se atoms like SnS_2 structure. The theoretical as well as experimental optimised lattice parameter for unit cell of $SnSe_2$ is reported to be 3.823 Å [29,30]. The lattice parameter for supercell increases proportionate to the size. Table 1 also shows the experimental value for lattice constant. In our calculations, a supercell of 2×2 $SnSe_2$ monolayer was constructed and the optimised lattice constant and bond-length were found to be 7.69 Å and 2.73 Å respectively. The 2×2 size of supercell was selected so as to provide necessary area for accommodating the alkali metal dopants. Also, many similar studies have been explored for various dichalcogenides and almost no effect is observed when supercell size is increased [15,31–35].

To enhance the electrocatalytic activity of $SnSe_2$, we doped S-block elements (Na, K and Ca) in the $SnSe_2$ monolayer. The doping concentration was set at 25% by substituting one Sn atom by Na, K and Ca respectively. As observed from Fig. 1, doping the monolayer with alkali metals does not distort $SnSe_2$ structure as the bond lengths between Na–Se (2.73 Å), K–Se (3.06 Å) and Ca–Se (2.86 Å) are found close to original bond length of $SnSe_2$. The maximum distortion in terms of bond-length is observed for K- doped $SnSe_2$; followed by Ca-doping. The bond length changes influence the electronegativity which in return modifies the work function.

The electronic density of states (DOS) play a vital role in understanding the electronic properties that further helps in selection of a good catalyst. For better electrocatalyst, generally a metallic system is highly preferred while a semiconducting system with band gap of around 1–2 eV is found suitable for photocatalyst or electro-photocatalyst. The DOS of any system also reveals the contribution of individual atoms of a system to the overall electronic transport and the underlying interaction of foreign atoms towards it. We have presented the electronic DOS for pristine and doped $SnSe_2$ in Fig. 2, which clearly show a band gap value of 0.8 eV for $SnSe_2$ that is in good agreement with previous work [19]. However, we can see from the figure that the substitution of Sn by different S group elements leads to a modification in electronic properties of pristine $SnSe_2$ and the system becomes metallic in nature. For a deeper insight into hydrogen (H) and oxygen (O) adsorption over these systems, we adsorbed H and O at the basal plane of $SnSe_2$ monolayer as well as on top site of the dopants as shown in Fig. 3(a and b) and evaluated the HER and OER activities (see Table 1).

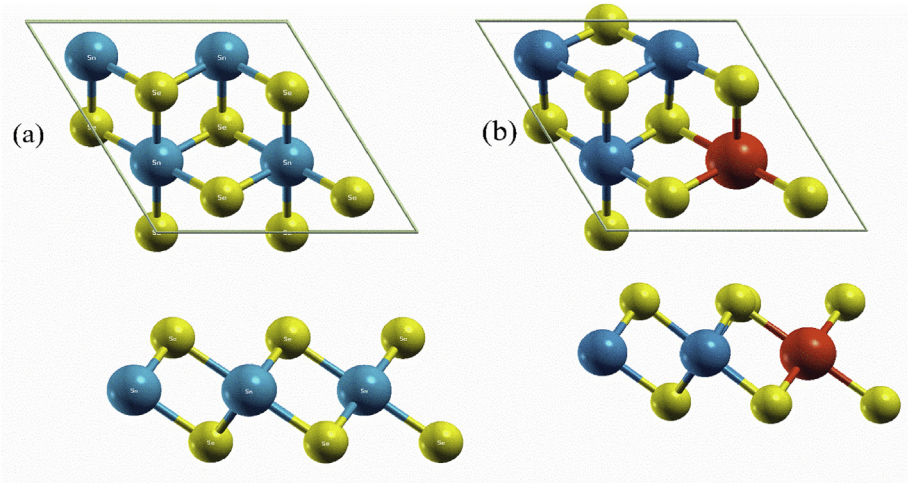

Fig. 1 – Top and side views of optimised geometries of (a) pristine $SnSe_2$ and (b) alkali metal doped-$SnSe_2$.

Please cite this article as: Inamdar AN et al., Hydrogen evolution and oxygen evolution reactions of pristine and alkali metal doped $SnSe_2$ monolayer, International Journal of Hydrogen Energy, https://doi.org/10.1016/j.ijhydene.2019.07.093

Table 1 – Optimised lattice constant, bond length, work function, adsorption energy and Gibbs free energy of hydrogen and oxygen of $SnSe_2$and alkali metal doped-$SnSe_2$. The value in parenthesis represent experimental value.

System	Lattice constant (Å)	Bond length (Å)	Work function φ(eV)	ΔE_H (eV)	ΔE_O (eV)	ΔG_H (eV)	ΔG_O (eV)
$SnSe_2$	7.659 (3.823)	2.73	5.95	0.55	−1.02	0.79	−0.69
Na-doped	7.501	2.73	5.91	−0.53	−0.87	−0.29	−0.54
K-doped	7.692	3.06	5.77	−1.53	−1.96	−1.29	−1.72
Ca-doped	7.597	2.86	6.10	0.48	−0.78	0.72	−0.45

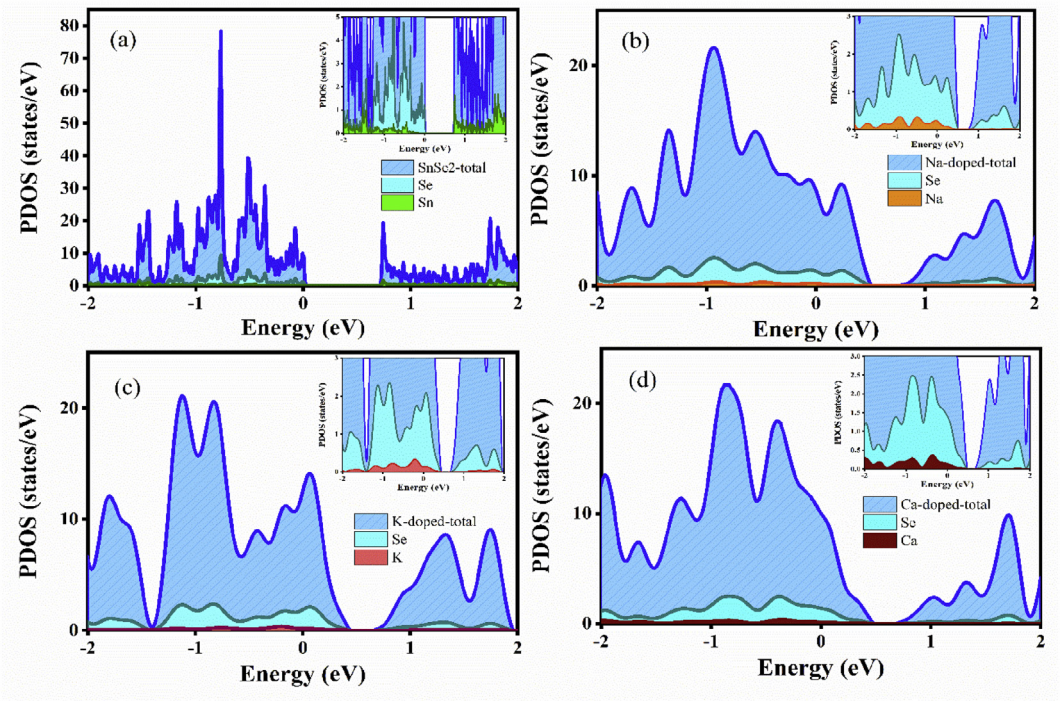

Fig. 2 – The density of states (DOS) of (a) pristine $SnSe_2$, (b) Na-doped $SnSe_2$, (c) K- doped $SnSe_2$ and (d) Ca-doped $SnSe_2$.

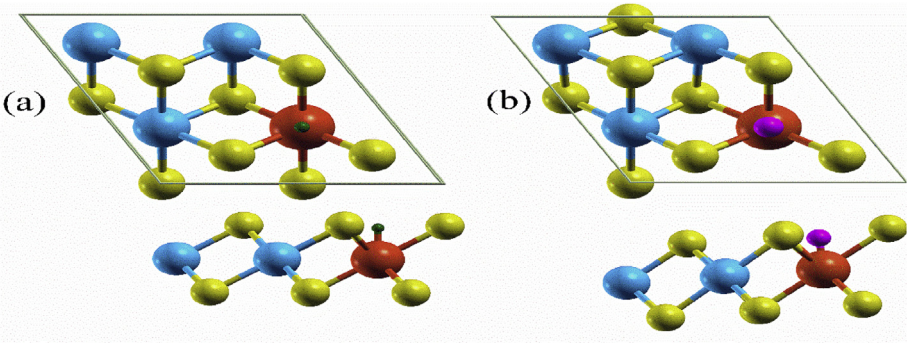

Fig. 3 – Top and side view of (a) hydrogen adsorbed and (b) oxygen adsorbed doped-$SnSe_2$.

To understand the effect of H and O adsorption on electronic transport of pristine and doped-$SnSe_2$, PDOS was computed and presented in Fig. 4(a) and (b). The partial DOS shows changes in electronic density of states of the systems due to strong interaction taking place between adsorbent and adsorbates. The higher contribution of density of states of H and O atoms present close to Fermi level leads their stronger adsorption over adsorbent.

The PDOS of hydrogen adsorbed pristine $SnSe_2$ monolayer (see Fig. 4(a)) show that the hydrogen contributes more to the conduction band (anti-bonding state) compared to the valence band regime (bonding state) near Fermi level indicating weak interaction with Sn atom resulting into physisorption. On the other hand, in case of alkali metal doped $SnSe_2$ monolayer, the PDOS plots reveal that the hydrogen contributes less in case of Na-doped $SnSe_2$ near Fermi level. This attributes that the hydrogen prefers to get adsorbed on the edge site that is to Se atoms than at the basal plane as the oxidation of Na is +1 whereas for Sn, it is +2 thereby leading to defect bonding in the Na-doped $SnSe_2$ monolayer. In case of K doped $SnSe_2$

Please cite this article as: Inamdar AN et al., Hydrogen evolution and oxygen evolution reactions of pristine and alkali metal doped $SnSe_2$ monolayer, International Journal of Hydrogen Energy, https://doi.org/10.1016/j.ijhydene.2019.07.093

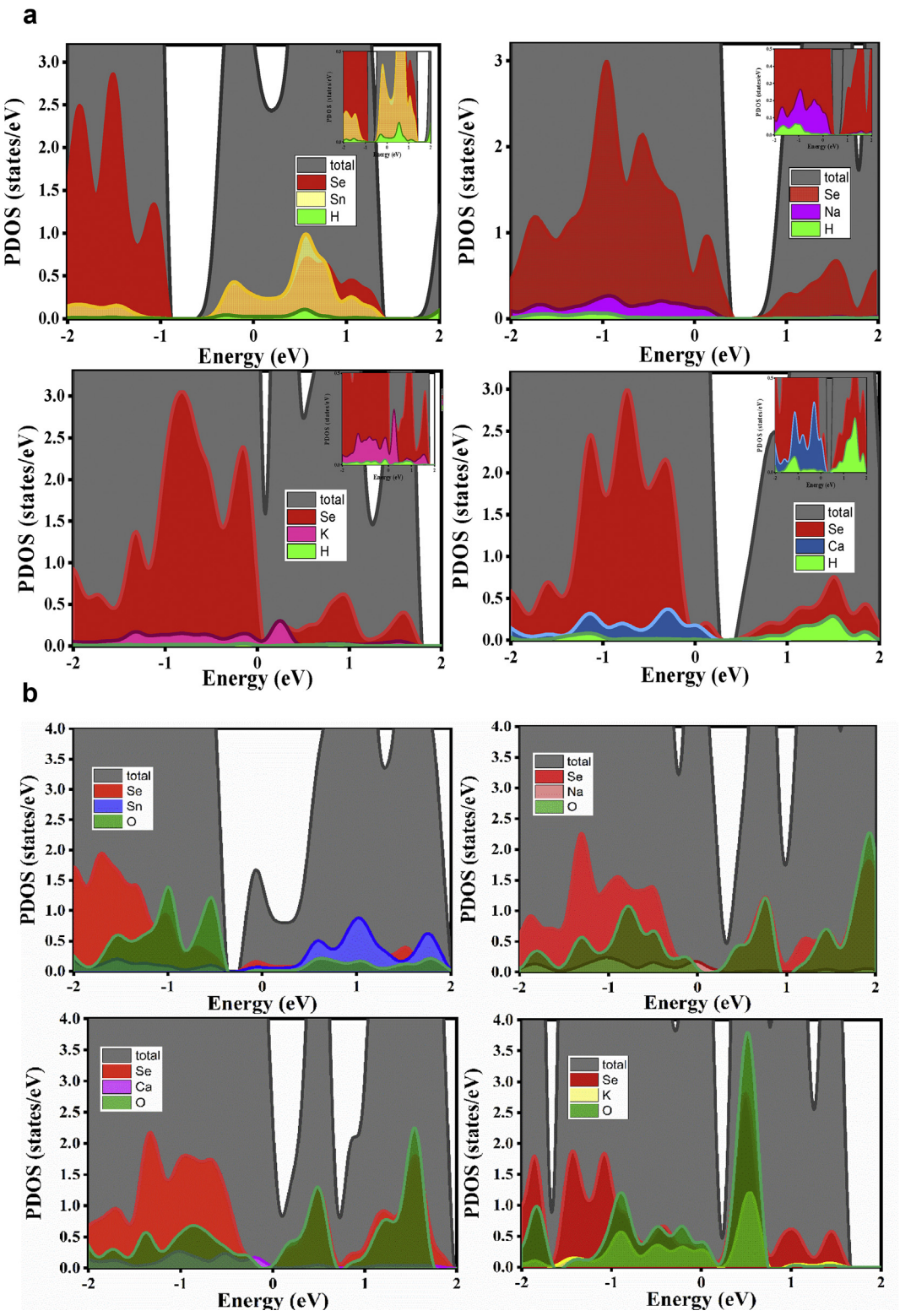

Fig. 4 – (a): Partial density of states (PDOS) of hydrogen adsorbed on $SnSe_2$and doped $SnSe_2$. (b): Partial density of states (PDOS) of oxygen adsorbed on $SnSe_2$and doped $SnSe_2$.

monolayer, the contribution of H atom towards valence band regime is significantly high which shows chemisorption due to strong interaction of hydrogen with K-doped $SnSe_2$ monolayer compared to other dopants. The contribution of H atom towards valence band in case of K and Na-doped $SnSe_2$ is due to the formation of defect bonds due to their +1 oxidation state. The H atom prefers Se edge-site than the basal plane and further enhances the contribution in valence band.

Please cite this article as: Inamdar AN et al., Hydrogen evolution and oxygen evolution reactions of pristine and alkali metal doped $SnSe_2$ monolayer, International Journal of Hydrogen Energy, https://doi.org/10.1016/j.ijhydene.2019.07.093

In case of Ca-doped $SnSe_2$, H atom contributs more in conduction band similar to the pristine $SnSe_2$ monolayer making it less suitable for HER catalyst. Further, we have also examined the charge transfer taking place during adsorption from pristine and doped-$SnSe_2$ to H and O atoms based on Lowdin charge analysis. We observed that there is electron accumulation on pristine and doped $SnSe_2$ of about 0.53e, 0.05e, 0.07e and 0.08e at Sn, Na, K and Ca atoms respectively during H adsorption, whereas during O adsorption, there is electron depletion at Sn, Na, K and Ca atoms of about 0.51e, 0.57e, 0.8e and 0.6e respectively. We found that during H adsorption, the electron accumulation is minimum in case of Na-dopant followed by K-dopant whereas on O adsorption, the electron depletion is minimum for pristine $SnSe_2$ followed by Ca dopant reflecting the relative differences in their electronegativity. The trends of oxygen and hydrogen interactions with the systems are distinct due to high electronegativity of oxygen than hydrogen. In case of oxygen adsorption, the $SnSe_2$ shows chemisorption unlike hydrogen adsorbed $SnSe_2$ as the contribution of oxygen in valence band regime is more than the conduction band regime that further results into a strong interaction between Sn and O. The contribution of oxygen near Fermi level is minimum in case of Ca doped $SnSe_2$ monolayer and hence, the interaction when compared to Na doped $SnSe_2$, suggests that the Ca-doped $SnSe_2$ monolayer is more suitable for OER catalyst. From our PDOS calculations (see Fig. 4), we conclude that the HER and OER catalytic activities are good for Na-doped and Ca-doped $SnSe_2$ monolayers respectively.

To examine the applicability of these systems as an electro-photo catalyst, we have calculated the absorption spectra of pristine and doped $SnSe_2$ monolayers. The optical absorption spectra provide fundamental information like highest absorption range and absorption co-efficient etc. of materials. Good electro-photocatalytic activity requires, E to be more than the sum of E_g and E_{AOP} (see equation (1)). From the absorption spectra, shown in Fig. (5), we can clearly observe that the $SnSe_2$ monolayer has an optical band gap of 1.2 eV. Further, doped $SnSe_2$ shows strong absorption peaks within the range 4–6.5 eV which means that the photons with high energy are required to excite the system. Therefore, all considered $SnSe_2$ systems can be utilized as high energy photo-electro catalyst.

We have also computed the work function (φ) of the systems to further support our obtained HER and OER results. The minimum amount of energy needed to remove an electron from the metal is known as work function. The work function and ionization energy are same if we consider the case of metals. The work function of a surface is strongly affected by the condition of the surface. It is a well-known fact that even with the small amount of contamination present in the monolayer leads to modification in surface reaction that further changes the magnitude of work function. The work function of the material can be defined as the energy difference between Fermi energy and vacuum level or electrostatic potential

$$\Phi = V_1 - E_F \tag{3}$$

Where φ is work function, V_1 is vacuum level or electrostatic potential and E_F is Fermi energy of the system. The computed work function of pristine and doped $SnSe_2$ monolayers is presented in Fig. 6. The graphs differ a lot in terms of the value of the Fermi energy and also the vacuum level. The change in the bond-length of K- doped $SnSe_2$ also can be depicted as we observe an asymmetrical behaviour of it as compared to all other cases. We can observe that the magnitude of work function decreases with incorporation of Na and K dopants; whereas doping with Ca atom results in an increase in the work function to 6.10 eV from the 5.95 eV (see Table 1). This increase can be attributed to the phenomenon of electronegativity. The electronegativity of Na, K and Ca-doped is 0.93, 0.82 and 1.00 respectively. The large value of electronegativity indicates that the elements are tightly bound and thus, it requires large amount of energy to excite it to the conduction band. Thus, the work function is elevated as compared to other two dopants. It is noteworthy that the magnitude of work function of pristine, Na and K doped $SnSe_2$ monolayers lies within the ranges of most effective HER catalysts platinum and palladium that have corresponding work functions of magnitudes 5.12 and 5.7 eV respectively [36]. This further confirms that the catalytic activity of Na- and Ca-doped $SnSe_2$ monolayer is good for HER and OER respectively.

Water electrolysis device is composed of a cathode-used as hydrogen evolution reaction catalyst on which water reduction takes place and an anode-used as oxygen evolution reaction catalyst [37]. Certain fixed amount of electrostatic potential is applied to these electrodes to split the water molecules into hydrogen and oxygen molecules. Regardless of the medium, the catalyst thermodynamic voltage is in general more than 1.23 V at 25 °C and 1 atm, which is considered as an overpotential to initiate the water-splitting procedure. It has been shown that the free energy of the hydrogen adsorbed state can be related to the exchange current density of HER, expressed as Sabatier relationship [38]. We have used Sabatier principle to investigate the HER and OER performances of the considered systems [39] that is characterized by free energy of adsorption of reactive intermediate on surface. Further, the exchange current density which is directly related to Gibbs free energy (ΔG) is utilized to determine the HER and OER catalytic efficiency of given catalyst surface under equilibrium condition [38]. The Gibbs free energy (ΔG) is expressed as follows:

$$\Delta G^x = \Delta E^X_{ads} + \Delta E^X_{ZPE} - T\Delta S^X \tag{4}$$

Where, X represents hydrogen or oxygen atom, E^X_{ads} is the adsorption energy of X atom adsorbed system and ΔE_{ZPE} represents the zero-point energy difference of X atoms in the adsorbed and gas phases and the term ΔS^X is the entropy of X. The corresponding Gibbs' Free energy of the hydrogen and oxygen adsorbed systems takes the following form: $\Delta G^H = E^H_{ads} + 0.24$ and $\Delta G^O = E^O_{ads} + 0.33$ respectively; as the terms ΔE^X_{ZPE} and $T\Delta S^X$ get reduced to 0.24 and 0.33 for hydrogen and oxygen adsorption respectively. The chemisorption energies of hydrogen and oxygen adsorption are defined as:

$$E^X_{ads} = E_{(system+X)} E_{(system)} - \frac{1}{2} E_{(X2)} \tag{5}$$

Where, $E_{(system+X)}$ is total energies of $SnSe_2$ or doped-$SnSe_2$ monolayer subjected to hydrogen or oxygen adsorption, $E_{(system)}$ is total energy of $SnSe_2$ or doped-$SnSe_2$ monolayer and

Please cite this article as: Inamdar AN et al., Hydrogen evolution and oxygen evolution reactions of pristine and alkali metal doped $SnSe_2$ monolayer, International Journal of Hydrogen Energy, https://doi.org/10.1016/j.ijhydene.2019.07.093

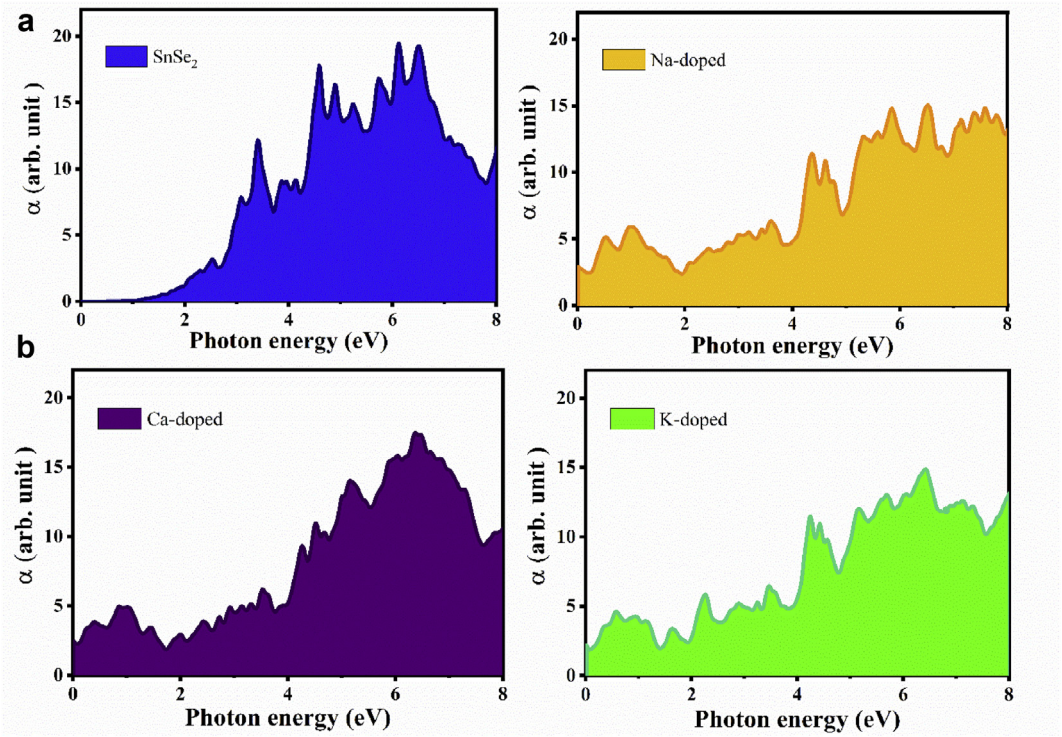

Fig. 5 – Top and side view of optimised geometric structure of (a) pristine $SnSe_2$ and (b) doped-$SnSe_2$.

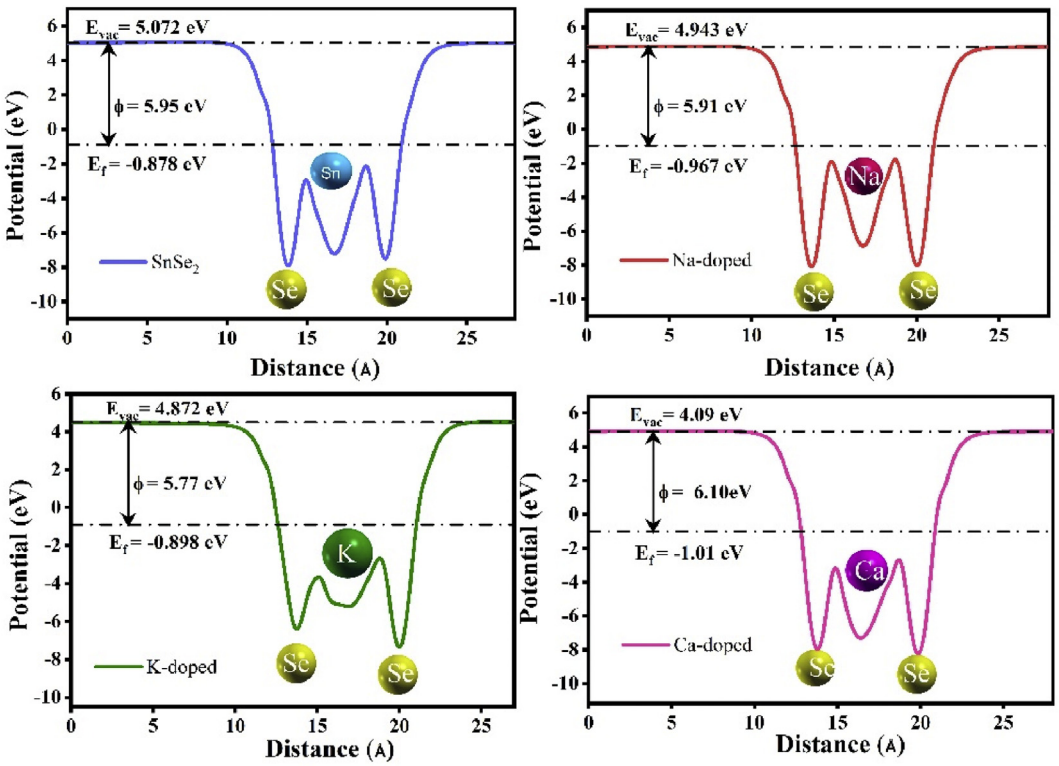

Fig. 6 – Work function of pristine $SnSe_2$ and doped-$SnSe_2$.

$E_{(X2)}$ stands for total energy of isolated hydrogen or oxygen molecule.

The best HER catalyst should have the magnitude of the Gibbs function ΔG^H close to zero. If the ΔG^H has high positive value, then H adsorption will be weaker such that the Volmer step of water-splitting becomes difficult; whereas, the high negative value of ΔG^H represents strong adsorption of the hydrogen on adsorbate that leads to difficulty in the

Please cite this article as: Inamdar AN et al., Hydrogen evolution and oxygen evolution reactions of pristine and alkali metal doped $SnSe_2$ monolayer, International Journal of Hydrogen Energy, https://doi.org/10.1016/j.ijhydene.2019.07.093

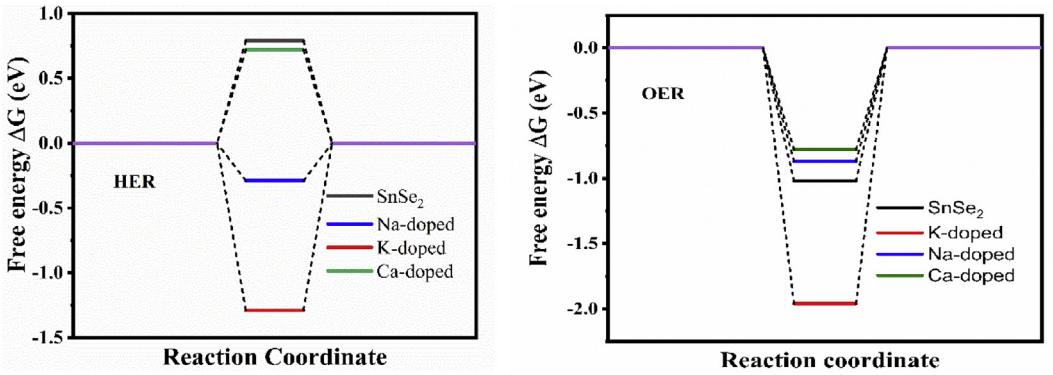

Fig. 7 – Reaction coordinate (a) HER and (b) OER of pristine $SnSe_2$ and doped-$SnSe_2$.

desorption of hydrogen molecule that makes the Heyrovsky or Tafel step difficult [40]. From the magnitude of the adsorption and Gibbs' free energy (see Table 1), we can say that the hydrogen strongly binds to K-doped $SnSe_2$ monolayer since, the value is too negative means desorption process will be difficult; whereas, in case of pristine and Ca-doped $SnSe_2$ monolayers, the positive values of both adsorption and Gibbs' energies tend to weaker hydrogen adsorption.

The Gibbs' energy of Na-doped $SnSe_2$ being least among all considered systems and is close to zero (see Fig. 7) for hydrogen adsorption, this indicates that the Na-doped $SnSe_2$ monolayer is best suited for HER catalytic activity. In case of oxygen adsorption, we found that the Ca-doped $SnSe_2$ monolayer shows good OER catalytic activity, followed by the Na-doped and pristine $SnSe_2$ monolayers. This can be attributed to the relative electronegativity of oxygen, which is more than that of hydrogen and this fact leads to different scenario of interaction.

Conclusion

In summary, we have systematically performed structural and electronic structure calculations of pristine and alkali atoms doped $SnSe_2$ monolayers using first-principles calculations based on density functional theory. Our computation on electronic density of states (DOS) reveals that the pristine $SnSe_2$ monolayer is semiconductor in nature, whereas after incorporation of alkali metal dopants, the monolayers transform to metallic nature. Site dependent hydrogen adsorption study was performed to analyse differences in adsorption capacities of the $SnSe_2$ monolayers with respect to different adsorption sites. We have observed that for pristine and Na doped-$SnSe_2$ monolayers, edge-site acts as most favourable site for hydrogen adsorption; whereas, for Ca and K-doped $SnSe_2$ monolayers, the basal plane show significant activity. In case of oxygen adsorption, the basal plane is found to be most preferential site for pristine and doped $SnSe_2$ monolayers. The Gibbs' free energy of these materials reveals them as a potential candidate to be utilized as a catalyst either for HER or OER. Our results show that the Na-doped $SnSe_2$ monolayer is more suited for HER catalyst as the Gibb's free energy is close to zero. The Ca-doped $SnSe_2$ monolayer is the better candidate for OER catalyst, followed by Na-doped and pristine $SnSe_2$ monolayers. In a nut-shell, we conclude that the over-all catalytic activity of the $SnSe_2$ monolayer can be significantly enhanced by a small amount of alkali metal dopants.

Acknowledgement

Authors are thankful to Department of Science and Technology (DST), New Delhi, India for funding. NS and PKJ are thankful to the INDO-SRILANKA bilateral project (Grant No.: DST/INT/SL/P-21/2016) for financial support. AI and AP are thankful to the DST PURSE Program (SR/PURSE Phase 2/28(C)) for financial support.

REFERENCES

[1] Turner JA. A realizable renewable energy future. Science 1999;285(5428):687–9. https://doi.org/10.1126/science.285.5428.687.
[2] Momirlan M, Veziroglu T. The properties of hydrogen as fuel tomorrow in sustainable energy system for a cleaner planet. Int J Hydrogen Energy 2005;30(7):795–802. https://doi.org/10.1016/j.ijhydene.2004.10.011.
[3] Bak T, Nowotny J, Rekas M, Sorrell C. Photo-electrochemical hydrogen generation from water using solar energy. Materials-related aspects. Int J Hydrogen Energy 2002;27(10):991–1022. https://doi.org/10.1016/s0360-3199(02)00022-8.
[4] Sørensen B, Spazzafumo G. Fuel cells. Hydrogen and Fuel Cells 2018:107–220. https://doi.org/10.1016/b978-0-08-100708-2.00003-5.
[5] Eftekhari A. Electrocatalysts for hydrogen evolution reaction. Int J Hydrogen Energy 2017;42(16):11053–77. https://doi.org/10.1016/j.ijhydene.2017.02.125.
[6] Li R, Li C. Photocatalytic water splitting on semiconductor-based photocatalysts. Adv Catal 2017:1–57. https://doi.org/10.1016/bs.acat.2017.09.001.
[7] Di J, Yan C, Handoko AD, Seh ZW, Li H, Liu Z. Ultrathin two-dimensional materials for photo- and electrocatalytic hydrogen evolution. Mater Today 2018. https://doi.org/10.1016/j.mattod.2018.01.034.
[8] Mascaretti L, Ferrulli S, Mazzolini P, Casari CS, Russo V, Matarrese R, Li Bassi A. Hydrogen-treated hierarchical titanium oxide nanostructures for photoelectrochemical

water splitting. Sol Energy Mater Sol Cells 2017;169:19–27. https://doi.org/10.1016/j.solmat.2017.04.045.
[9] Kumar DP, Kumari VD, Karthik M, Sathish M, Shankar MV. Shape dependence structural, optical and photocatalytic properties of TiO_2 nanocrystals for enhanced hydrogen production via glycerol reforming. Sol Energy Mater Sol Cells 2017;163:113–9. https://doi.org/10.1016/j.solmat.2017.01.007.
[10] Alizadeh M, Tong GB, Mehmood MS, Qader KW, Rahman SA, Shokri B. Band engineered Al-rich InAlN thin films as a promising photoanode for hydrogen generation from solar water splitting. Sol Energy Mater Sol Cells 2018;185:445–55. https://doi.org/10.1016/j.solmat.2018.05.058.
[11] Sathe BR, Zou X, Asefa T. Metal-free B-doped graphene with efficient electrocatalytic activity for hydrogen evolution reaction. Catal Sci Technol 2014;4(7):2023–30. https://doi.org/10.1039/c4cy00075g.
[12] Dolganov AV, Tarasova OV, Ivleva AY, Chernyaeva OY, Grigoryan KA, Ganz VS. Iron (II) clathrochelates as electrocatalysts of hydrogen evolution reaction at low pH. Int J Hydrogen Energy 2017;42(44):27084–93. https://doi.org/10.1016/j.ijhydene.2017.09.080.
[13] Mir SH, Chakraborty S, Jha PC, Wärnå J, Soni H, Jha PK, Ahuja R. Two-dimensional boron: lightest catalyst for hydrogen and oxygen evolution reaction. Appl Phys Lett 2016;109(5). https://doi.org/10.1063/1.4960102. 053903.
[14] Mir SH, Chakraborty S, Wärnå J, Narayan S, Jha PC, Jha PK, et al. A comparative study of hydrogen evolution reaction on pseudo-monolayer WS_2 and PtS_2: insights based on the density functional theory. Catal Sci Technol 2017;7(3):687–92. https://doi.org/10.1039/c6cy02426b.
[15] Som NN, Mankad V, Jha PK. Hydrogen evolution reaction: the role of arsenene nanosheet and dopant. Int J Hydrogen Energy 2018. https://doi.org/10.1016/j.ijhydene.2018.03.066.
[16] Pillai SB, Dabhi SD, Jha PK. Hydrogen evolution reaction and electronic structure calculation of two dimensional bismuth and its alloys. Int J Hydrogen Energy 2018. https://doi.org/10.1016/j.ijhydene.2018.04.009.
[17] Kubisztal J, Budnio A, Lasia A. Study of the hydrogen evolution reaction on nickel-based composite coatings containing molybdenum powder. Int J Hydrogen Energy 2007;32(9):1211–8. https://doi.org/10.1016/j.ijhydene.2006.11.020.
[18] Gao M-R, Chan MKY, Sun Y. Edge-terminated molybdenum disulfide with a 9.4-Å interlayer spacing for electrochemical hydrogen production. Nat Commun 2015;6(1). https://doi.org/10.1038/ncomms8493.
[19] Wu X, Han J, Feng Y, Li G, Wang C, Ding G, et al. Half-metals and half-semiconductors in a transition metal doped $SnSe_2$ monolayer: a first-principles study. RSC Adv 2017;7(70):44499–504. https://doi.org/10.1039/c7ra07648g.
[20] Sun C, Zhang J, Ma J, Liu P, Gao D, Tao K, et al. N-doped WS_2 nanosheets: a high-performance electrocatalyst for the hydrogen evolution reaction. J Mater Chem 2016;4(29):11234–8. https://doi.org/10.1039/c6ta04082a.
[21] Long G, Wan K, Liu M, Liang Z, Piao J, Tsiakaras P. Active sites and mechanism on nitrogen-doped carbon catalyst for hydrogen evolution reaction. J Catal 2017;348:151–9. https://doi.org/10.1016/j.jcat.2017.02.021.
[22] Dong S, Wang Z. Improving the catalytic activity for hydrogen evolution of monolayered $SnSe_{2(1-x)}S_{2x}$ by mechanical strain. Beilstein J Nanotechnol 2018;9:1820–7. https://doi.org/10.3762/bjnano.9.173.
[23] Wang L, Chen X, Du H, Yuan Y, Qu H, Zou M. First-principles investigation on hydrogen storage performance of Li, Na and K decorated borophene. Appl Surf Sci 2018;427:1030–7. https://doi.org/10.1016/j.apsusc.2017.08.126. 2018.
[24] Reunchan P, Jhi S-H. Metal-dispersed porous graphene for hydrogen storage. Appl Phys Lett 2011;98(9). https://doi.org/10.1063/1.3560468. 093103.
[25] Li Y, Ding X, Zhang Q. Self-printing on graphitic nanosheets with metal borohydride nanodots for hydrogen storage. Sci Rep 2016;6(1). https://doi.org/10.1038/srep31144.
[26] Giannozzi P, Baroni S, Bonini N, Calandra M, Car R, Cavazzoni C, Wentzcovitch RM. Quantum espresso: a modular and open-source software project for quantum simulations of materials. J Phys Condens Matter 2009;21(39):395502. https://doi.org/10.1088/0953-8984/21/39/395502.
[27] Perdew JP, Burke K, Wang Y. Generalized gradient approximation for the exchange-correlation hole of a many-electron system. Phys Rev B 1996;54(23):16533–9. https://doi.org/10.1103/physrevb.54.16533.
[28] Monkhorst HJ, Pack JD. Special points for Brillouin-zone integrations. Phys Rev B 1976;13(12):5188–92. https://doi.org/10.1103/physrevb.13.5188.
[29] Gonzalez JM, Oleynik. Layer-dependent properties of SnS_2 and $SnSe_2$ two-dimensional materials. Phys Rev B 2016;94(12). https://doi.org/10.1103/physrevb.94.125443.
[30] Schlüter M, Cohen ML. Valence-band density of states and chemical bonding for several non-transition-metal layer compounds: $SnSe_2$, PbI_2, BiI_3, and GaSe. Phys Rev B 1976;4(2):424–31. https://doi.org/10.1103/physrevb.14.424.
[31] Ma S, Yuan D, Jiao Z, Wang T, Dai X. Monolayer Sc_2CO_2: a promising candidate as a SO_2 gas sensor or capturer. J Phys Chem C 2017;121(43):24077–84. https://doi.org/10.1021/acs.jpcc.7b07921.
[32] Yu X, Li Y, Cheng J, Liu Z, Li Q, Li W, et al. Monolayer Ti_2CO_2: a promising candidate for NH_3 sensor or capturer with high sensitivity and selectivity. ACS Appl Mater Interfaces 2015;7(24):13707–13. https://doi.org/10.1021/acsami.5b03737.
[33] Othman MA, Ahmad BH, Amat NF. An overview of nanonet based dye-sensitized solar cell (DSSC) in solar cloth. JSTS: J Semicond Technol Sci 2013. https://doi.org/10.5573/JSTS.2013.13.6.635.
[34] Upadhyay D, Roondhe B, Pratap A, Jha PK. Two-dimensional delafossite cobalt oxyhydroxide as a toxic gas sensor. Appl Surf Sci 2019. https://doi.org/10.1016/j.apsusc.2019.01.057.
[35] Chou SS, Sai N, Lu P, Coker EN, Liu S, Artyushkova K, Brinker CJ. Understanding catalysis in a multiphasic two-dimensional transition metal dichalcogenide. Nat Commun 2015;6(1). https://doi.org/10.1038/ncomms9311.
[36] Michaelson HB. The work function of the elements and its periodicity. J Appl Phys 1977;48(11):4729–33. https://doi.org/10.1063/1.323539.
[37] Coutanceau C, Baranton S, Audichon T. Hydrogen production from water electrolysis. Hydrogen Electrochemical Production 2018:7–62. https://doi.org/10.1016/b978-0-12-811250-2.00003-0.
[38] Nørskov JK, Bligaard T, Logadottir A, Kitchin JR, Chen JG, Pandelov S, Stimming U. Trends in the exchange current for hydrogen evolution. J Electrochem Soc 2005;152(3). https://doi.org/10.1149/1.1856988. J23.
[39] Greeley J, Jaramillo TF, Bonde J, Chorkendorff I, Nørskov JK. Computational high-throughput screening of electrocatalytic materials for hydrogen evolution. Nat Mater 2006;5(11):909–13. https://doi.org/10.1038/nmat1752.
[40] Ding Q, Song B, Xu P, Jin S. Efficient electrocatalytic and photoelectrochemical hydrogen generation using MoS_2 and related compounds. Chem 2016;1(5):699–726. https://doi.org/10.1016/j.chempr.2016.10.007.

Please cite this article as: Inamdar AN et al., Hydrogen evolution and oxygen evolution reactions of pristine and alkali metal doped $SnSe_2$ monolayer, International Journal of Hydrogen Energy, https://doi.org/10.1016/j.ijhydene.2019.07.093

International Journal of Hydrogen Energy 68 (2024) 268–276

Contents lists available at ScienceDirect

International Journal of Hydrogen Energy

journal homepage: www.elsevier.com/locate/he

A striking exploration of defect engineering in HfS_2, $HfSe_2$, and janus HfSSe through ab initio analysis for HER catalysis application

Archana N. Inamdar [a], Narayan N. Som [c], Shweta Dabhi [d], Arun Pratap [a], Piotr Spiewak [e], Krzysztof Kurzydłowski [f], Prafulla K. Jha [b,*]

[a] Department of Applied Physics, Faculty of Technology and Engineering, The Maharaja Sayajirao University of Baroda, Vadodara, 390001, India
[b] Department of Physics, Faculty of Science, The Maharaja Sayajirao University of Baroda, Vadodara, 390002, India
[c] Institute of High-Pressure Physics, Polish Academy of Sciences, Sokolowska 29/37, 01-142, Warsaw, Poland
[d] Department of Physical Sciences, P. D. Patel Institute of Applied Science, CHARUSAT Campus, Changa, Gujarat, 388421, India
[e] Faculty of Materials Science and Engineering, Warsaw University of Technology, Wołoska 141, 02-507, Warsaw, Poland
[f] Faculty of Mechanical Engineering, Białystok University of Technology, Wiejska 45C, 15-351, Białystok, Poland

ARTICLE INFO

Handling Editor: Dr M Djukic

Keywords:
Transition metal dichalcogenides
Janus materials
Density functional theory (DFT)
Hydrogen evolution reaction (HER)

ABSTRACT

The present study emphasizes the enhancement in catalytic activity due to the formation of vacancies using dispersion corrected density functional theory. We observed that without vacancy formation, in general the edge site is an active site for hydrogen adsorption, while the lowest Gibbs free energy (ΔG^H) is found to be for Janus HfSSe at the S-edge site. Furthermore, interestingly, due to the hindrance of the edge site, it facilitates only the Volmer-Heyrovsky reaction rather than the Volmer-Tafel. Among the mono vacancies, the Hafnium mono vacancy shows the lowest adsorption energy.

We observed a competition between the evolution of H_2S and H_2 gas in the case of HfS_2-V_{Hf}, whereas in the case of defected Janus and $HfSe_2$, due to the presence of Se layers, we observed no competitiveness with H_2S or H_2Se gas with hydrogen gas. These defected materials exhibit lower reactional Gibbs free energy than a pristine monolayer due to its metallic nature. We observed that Hafnium vacancy enhances the HER activity, and pave the way for dominating Volmer-Heyrovsky reaction.

1. Introduction

Energy is the most basic requirement for the survival and progress of mankind [1,2]. However, the extensive demand of energy and rapid extinction of non-renewable fossil fuels and hazardous effects of these fossil fuels on the environment leads to the search of clean energy sources such as biomass, geothermal, solar, hydro and tidal energy [3–6]. Among the clean energy sources available, hydrogen energy has emerged as one of the most promising alternatives to fossil fuels due to its high gravimetric specific energy density and environmentally friendly characteristics which has its use in many other industries [7,8]. Production of hydrogen using conventional methods is not as promising due to the high standards for energy sustainability. Therefore, the development of green and clean technologies to boost the hydrogen economy is of paramount importance [12]. Out of other methods available to produce hydrogen, the electrochemical splitting of water (using photocatalyst/electrocatalyst/photoelectron catalyst) has gained significant attention due to its carbon-free hydrogen generation [9–11]. In the electrochemical splitting of water, hydrogen gas (H_2) is the by-product of water electrolysis, in which catalysts play a pivotal role [13]. In this method, the water splitting procedure can be subdivided into two half reactions: the evolution of H_2 that is represented by Ref. [14],

$$2H^+ + 2e^- \rightarrow H_2 \quad (1)$$

and evolution of oxygen gas (O_2) that is,

$$2H_2O \rightarrow 4H^+ + 4e^- + O_2 \quad (2)$$

The Hydrogen Evolution Reaction (HER) involves a two-electron transfer process with the involvement of a catalytic intermediate, reaction called Volmer reaction. Noble metals such as Pt, Pd, Au, Ag etc. catalyze the electrochemical generation of hydrogen at ultralow overpotential values [14,15], but their high price and scarcity are major

* Corresponding author.
E-mail addresses: pk.jha-phy@msubaroda.ac.in, prafullaj@yahoo.com (P.K. Jha).

https://doi.org/10.1016/j.ijhydene.2024.04.143
Received 30 September 2023; Received in revised form 9 April 2024; Accepted 11 April 2024
Available online 26 April 2024

drawbacks. Therefore, the discovery of earth abundant HER catalysts with very low overpotentials is highly desirable [16,17]. Among all the available materials, transition metal dichalcogenides (TMDs) have attracted wide attention due to their low cost and high HER activity [18–20]. The HER performance of two-dimensional (2D) TMD electrocatalysts is reported to be better than that of commercial benchmark Pt/C catalysts at high current densities which is a promising factor in industrial hydrogen production [21,22]. The molecular structure of 2D TMDs is of MX_2 type, where M is a transition metal atom (e.g Mo, W, Zr, Sn etc.) and X is a chalcogen atom (e.g S, Se and Te). The TMDs exist in various structural phases among which 2H and 1T phases are the most common [14]. The diversity in their structural phases makes it possess a wealth of electronic, magnetic and optical properties [14]. The 2D TMDs such as MoS_2, WS_2, $SnSe_2$ have attracted humongous attention for its low-cost fabrication and better electrocatalytic activity [23]. However, it is observed that the basal plane of TMDs is less reactive as compared to edge sites restricting its maximum use [23]. To improve this drawback there are many ways such as doping, defect and application of strain.

Defect chemistry within two-dimensional (2D) materials encompasses various types of imperfections, including edge defects, topological defects, vacancies, and dopant-derived defects. These defects hold significant importance in electrocatalysis because they often serve as active sites actively participating in chemical reactions. Additionally, defects can influence the electronic structure of active sites and promote the exposure of more catalytic sites to the electrolyte [24–27]. Consequently, defect engineering has emerged as a highly promising approach for finely tuned electrocatalytic performance [24,25,28]. Among the widely spread materials, there are quite a few studies on HfX_2 (where X = S, Se, Te) compounds [29–37]. The observations from the study reveal that the HfX_2 compounds have a reasonably low bandgap and mobility which makes it a suitable candidate for electronic and optoelectronic applications [38–40]. The electrochemical activation of $ZrSe_2$ and $HfSe_2$ towards HER takes place via both oxidation and reduction [29–31]. Further, the investigation of the enhancement in structural, electronic and optical properties of HfS_2 monolayer via doping of lathanide atoms is carried out [32–34]. There are studies on the Janus structure of S and Se in HfSSe for its application in electronic devices [35–37]. We found that these show vast applications of the materials, which led us to investigate the properties of three compounds $HfSe_2$, HfS_2 and HfSSe via defect engineering. Numerous studies have shown promise in utilizing defect engineering techniques to enhance the catalytic performance of Janus materials such as WSSe, $MoSi_2N_4$, $MoSiGeN_4$ and $WSiGeN_4$ [41,42]. For example, Dequan et al. [41] investigated the impact of intrinsic strain resulting from the janus structure and the role of vacancies in activating the inert basal plane. They found an optimal hydrogen adsorption free energy (ΔG^H) close to thermoneutrality in the WSSe system, achieving high HER catalytic activity under strain-free conditions with the presence of S/Se vacancies at their intrinsic concentrations. Additionally, Yadong et al. conducted first-principles calculations to systematically explore the structural, electronic, optical and photocatalytic properties of emerging materials like $MoSi_2N_4$, as well as proposed janus structures such as $MoSiGeN_4$ and $WSiGeN_4$. Their results confirmed the suitability of these janus structures for HER activity [42]. Wang et al. conducted a comprehensive study on the properties of 2D HfS_2, revealing its impressive characteristics such as a suitable bandgap, high carrier mobility, remarkable sheet current density, and robust chemical stability. These attribute 2D HfS_2 as a promising material for diverse applications [43]. In similar manner, Yao et al. [44] explored the characteristics of 2D $HfSe_2$, focusing on the structure and density of various defects prevalent on the $HfSe_2$ surface. They utilized scanning tunneling microscopy and spectroscopy for their analysis. Despite similarities with defects found in MoS_2 and WSe_2, $HfSe_2$ is distinguished by a significantly higher defect density of approximately 9×10^{11} cm^{-2}. Its suitability for use in transition metal dichalcogenide-based field-effect transistors is underscored by its moderate band gap of around 1 eV and the high-κ dielectric properties of its native oxide. Additionally, Hoat et al. [37] delved into the Janus HfSSe monolayer, employing first-principles calculations through the full-potential linearized augmented plane-wave (FP-LAPW) method. Their findings confirmed the dynamic stability of the HfSSe Janus monolayer, which is characterized as an indirect gap semiconductor. Bera et al. [45] also contributed to this field by analyzing the phonon structures of HfS_2, $HfSe_2$, and Janus HfSSe and confirmed the dynamical stability of these materials. Given the existence of studies that demonstrate positive phonon dispersion curves and thereby affirm the stability of these materials, we have chosen not to conduct these calculations within our paper. This decision is based on the substantial evidence already available, which we believe sufficiently supports our findings without necessitating further computational validation in this area.

In our present work, structural and electronic properties along with catalytic activity for HER of all three structures i.e $HfSe_2$, HfS_2 and HfSSe have been explored. We are further motivated to tune the fundamental properties such as structural and electronic, as well as the catalytic performance with the creation of various defects. Both the required mechanisms for water-splitting process are explored, the initial Volmer reaction which is followed by Tafel and Heyrovsky reactions. All the calculations were performed with the use of dispersion-corrected (D2) density functional theory (DFT).

2. Computational methodology

2.1. Computational details

In this article, the structural, electronic and catalytic properties of pristine and defected $HfSe_2$, HfS_2 and HfSSe monolayers were performed using state-of-art first-principles based density functional theory (DFT) as implemented in Quantum Espresso code [46]. The exchange correlation interaction was treated within the generalized gradient approximation (GGA) proposed by Perdew-Burke-Ernzerhof (PBE) [47]. Further, the dispersion correction (D2) of Grimme has been employed throughout the calculation to get accurate value of adsorption energy for hydrogen adsorption [48]. A $3 \times 3 \times 1$ supercell of all structures are considered so that the surface area is large enough to obtain acceptable result. The kinetic energy and charge density cut-offs are 80 and 800 Ry respectively which are sufficient to fully converge lattice parameters and total energy within the specified threshold criterion. To avoid interaction between two successive layers, a distance of 15 Å is inserted perpendicular to monolayer. The reciprocal space was sampled by a dense grid of $7 \times 7 \times 1$ constructed under Monkhorst-Pack scheme [49]. The Marzari-Vanderbilt smearing has been employed for required calculations. The energy convergence value between two consecutive steps was chosen as 10^{-4} eV and convergence was repeated self consistently until the maximum Hellmann-Feynman forces acting on each atom were less than 0.001 eV/Å. To acquire an energy convergence threshold of 1×10^{-8} Ry by solving Kohn-Sham equation, an iterative Davidson type diagonalization approach was used.

2.2. Theoretical formulations

The HER activity of pristine and defected $HfSe_2$, HfS_2 and HfSSe monolayers, are investigated according to the Sabatier principle [3–6]. The Sabatier principle states that, the reaction between catalysts and intermediates should be just right neither strong nor weak. At equilibrium condition, efficiency of HER activity at given surface is determined by exchange current density which is related to change in Gibbs free energy of H-adsorption (ΔG^H) [50–52] at (pH = 0) and can be defined as follows:

$$\Delta G^H = \Delta E^H_{ads} + \Delta E_{ZPE} - T\Delta S \quad (3)$$

Here ΔE^H_{ads} is the adsorption energy of hydrogen (H) atom. The entropy of adsorption of $\frac{1}{2}H_2$ is $\Delta S \cong -\frac{1}{2}S^0_{H_2}$ as the vibrational entropy in

the adsorbed state is relatively small [50–52]. Where $S^0_{H_2}$ is the entropy of H_2 in the gas phase at standard conditions. The Gibbs free energy is calculated using the obtained TΔS which is −0.2 eV and ΔE_{ZPE} using the following equation.

$$\Delta E_{ZPE} = E^H_{ZPE} - \frac{1}{2}E^{H_2}_{ZPE} \quad (4)$$

where, E^H_{ZPE} and $E^{H_2}_{ZPE}$ is the zero-point energy of atomic hydrogens on the catalyst and H_2 in gas phase respectively. The obtained value of E_{ZPE} - TΔS is listed in ***Tabel 2*** and Table 3. The hydrogen adsorption energy (ΔE^H_{ads}) is defined as,

$$\Delta E^H_{ads} = E(system + H) - E(system) - ½\,E(H_2) \quad (5)$$

where E (system + H) is total energy of hydrogen adsorbed pristine or defected systems, E(system) is the energy of pristine or defected systems without adsorption, $E(H_2)$ is the energy of isolated hydrogen molecule. The best catalyst platinum has ΔG^H close to zero. Therefore, for excellent catalytic activity of HER, ΔG^H should be zero or close to zero. According to the Sabatier principle, if hydrogen (H) binds weakly to the surface (i.e., ΔG^H is too positive), it will result in difficulty during the adsorption step. Conversely, if hydrogen binds strongly (i.e., ΔG^H is too negative) to the surface, it will lead to difficulty during the desorption step. Therefore, achieving an optimal ΔG^H is crucial for ensuring excellent catalytic activity in the hydrogen evolution reaction (HER). In addition, two other descriptors for HER activity are the overpotential and exchange current density and given by following relation [52].

$$\eta = \Delta G^H/e \quad (6)$$

$$i_0 = -eK_0 \frac{1}{1 + e^{\frac{|\Delta G^H|}{K_B T}}} \quad (7)$$

Where e is electron charge, K_B is Boltzmann constant (eV/K), T = 298 K and rate constant $K_0 = 1\ s^{-1}\ site^{-1}$.

3. Results and discussion

3.1. Structural properties of pristine structures

In the present work, we have studied the structural, electronic and catalytic properties of 3 × 3 × 1 supercell of pristine 1T-phase HfS_2, $HfSe_2$ and Janus structure HfSSe along with various defects. When considering Janus HfSSe, a unique scenario arises where one of the chalcogen layers within the original HfX_2 TMD monolayer is substituted with a layer containing atoms of a different type. To illustrate, the S layer in HfS_2 gets replaced with Se, or vice versa. The substitution or change made to the structure, and this change has a noticeable impact. Specifically, the change disrupts the symmetry of the structure along the vertical axis, making it less balanced or uniform. This loss of balance affects the overall symmetry of the P-3m1 space group, meaning that the structure is no longer as symmetrical as it was before the substitution.

The top and side views of the HfS_2, $HfSe_2$ and Janus HfSSe are pictorially represented in Fig. 1. The optimized lattice constants for the monolayers HfS_2, $HfSe_2$ and HfSSe are 10.99 Å, 11.22 Å and 11.11 Å respectively, which have nice accordance with previous studies [45,53]. The bond-lengths between Hf–S and Hf–Se are 2.56 Å and 2.68 Å respectively and for Janus HfSSe the bond-lengths Hf–S is 2.56 Å and Hf–Se is 5.69 Å as depicted in Table 1 which are consistent with previous reports [45].

The structural stability of 1T phase of $HfSe_2$, HfSSe, and HfS_2 have been confirmed elsewhere through formation energy, phonon dispersion curve, and/or AIMD simulation [54]. It is also shown that the 1T phase exhibits higher relative phase stability than the 2H phase. The calculated formation agrees with the previous report [37–40,54–56]. After the confirmation of the phase stability of the considered systems, we further investigate its electronic and catalytic activity.

3.2. Electronic properties of pristine structures

The calculated band structure of pristine HfS_2, $HfSe_2$ and Janus HfSSe are shown in Fig. 2. In all three monolayers, namely HfS_2, $HfSe_2$, and Janus HfSSe, the highest energy level in the valence band, known as the valence band maxima (VBM), is situated at the high symmetry point Γ of Brillouin zone. Conversely, the lowest energy level in the conduction band, referred to as the conduction band minima (CBM), is found at the high symmetry point M. This arrangement gives rise to an indirect bandgap in these materials. The band gap of HfS_2, $HfSe_2$ and Janus HfSSe is found to be 1.56 eV, 0.68 eV and 1.04 eV respectively which are very well in accordance with the previous reports [45]. The PBE functional underestimates the band gap, the previously reported band gap of HfS_2 and $HfSe_2$ is found to be 2.40 and 1.32 eV respectively with the HSE06 functional [57,58]. It is interesting to note that the Janus HfSSe exhibits band gap in between the HfS_2 and $HfSe_2$. The band gap of HfSSe decreases due to incorporation of Se atoms in place of S atoms. The band gap of HfS_2, $HfSe_2$ and HfSSe lies in the range of 1.2–2.5 eV, which makes them potential candidates for photo-catalyst. As discussed earlier, Pt is metallic in nature and exhibits excellent candidate for HER but limited abundance limits its large-scale application. However, searching for cheap and easily available catalysts are highly demanded [59–62].

Table 1
Calculated lattice, bond lengths and Formation energy of HfS_2, $HfSe_2$ and HfSSe monolayers.

Systems	Lattice (Å)	Bond length (Å)	E_{form} (eV)
HfS_2	10.99	2.56	−4.80
$HfSe_2$	11.22	2.68	−4.03
HfSSe	11.11	2.56 (Hf–S) 5.69 (Hf–Se)	−4.41

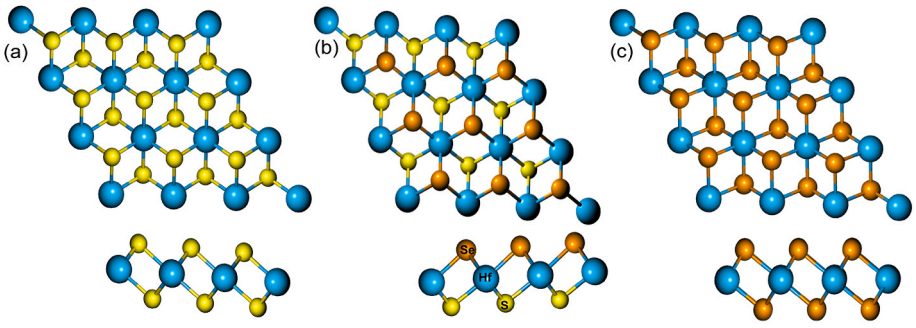

Fig. 1. The optimized geometries of (a) HfS_2, (b) HfSSe and (c) $HfSe_2$ monolayers.

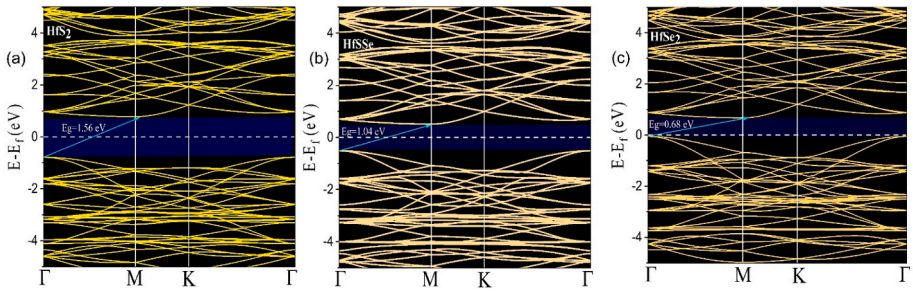

Fig. 2. Band structure of pristine (a) HfS_2, (b) HfSSe and (c) $HfSe_2$ monolayers.

3.3. Catalytic properties of pristine structures

It is observed through the various studies that edge sites of the TMDs is more efficient in terms of catalysis as compared to basal plane [63]. Chalcogen elements, such as S and Se, positioned at the edges of 2D materials, present unsaturated bonds due to the crystal structure ending at these points. This results in a higher level of reactivity at the edge sites compared to the atoms in the basal plane. This heightened reactivity is critical for various applications, including catalysis, as well as energy storage and conversion technologies, where the process of molecules attaching and detaching from the material's surface is essential. Specifically, the superior performance of TMDs in facilitating HER is often credited to the advantageous adsorption sites formed by S or Se atoms located at the edges [64–66]. Thus, we have studied H adsorption on various sites of these pristine structures.

Fig. 3 depicts the optimized structures after H-adsorption over HfS_2, $HfSe_2$ and HfSSe. We have calculated ΔE^{H}_{ads} and ΔG^{H} at various sites of these monolayers using equations (3) and (5). The values are shown in Table 2. Here, as observed from the table, in case of HfS_2 the S edge adsorption shows better catalytic activity as compared to basal plane. Similarly, in case of $HfSe_2$ we observe the same trend of active edge site compared to basal plane. Also, it is evident that HfS_2 has better catalytic efficiency than $HfSe_2$ as this trend has been observed in case of ZrS_2 and $ZrSe_2$ also [67]. Additionally, when we contrast HfS_2 with $HfSe_2$, we observe that the sulphur edge exhibits greater reactivity in comparison to the selenium edge. Interestingly, this differs from the general trend seen in transition metal dichalcogenides (TMDs), where selenium-based catalysts tend to be more active than their sulphur counterparts [63]. In the context of Janus structures, there exist two distinct edge sites: one composed of sulphur atoms, referred to as the S-edge, and the other consisting of selenide atoms, known as the Se-edge. It is evident that because of the highly asymmetric arrangement of atoms in Janus configurations, there is an augmentation in catalytic activity specifically at the edges. Additionally, it's worth noting that Janus structures exhibit a rather unconventional trend, where the sulphur edge site displays higher reactivity compared to the selenide edge. Finally, we can evaluate from comparison of Gibbs free energy of all three systems at basal plane and edge site, which yields us the following sequence SHfSe > HfS_2 > $HfSe_2$ where SHfSe refers to the hydrogen adsorption at S-edge site. The Janus structure yields good catalytic activity for HER, as observed in Janus SeMoS [68]. The hydrogen adsorption is in following sequence HfSSe > HfS_2 > $HfSe_2$. The Lowdin charge analysis explains, the charge transfer mechanism from catalyst to hydrogen, in Table 2, we can clearly observe increment in the charge of hydrogen atom which is attributed charge transfer from the system to hydrogen atom. If ΔQ_H (e) (difference in charge hydrogen before and after adsorption) is positive means charge transfer from the system to hydrogen and negative means charge transfer from hydrogen atom to system. Comparing the ΔQ_H of HfS_2 and $HfSe_2$, ΔQ_H is higher for HfS_2 which is the reason that HfS_2 is better catalyst for HER. However, in the case of the Janus, due to charge redistribution of S and Se due to asymmetric arrangement, the ΔQ_H value for Se site is higher than S site, which is core reason for enhancement of Se site in Janus system as compared to the pristine counterpart. The löwdin charge analysis validated the results obtained from the ΔG^{H} and ΔE^{H}_{ads}. We observed, there is higher transfer at basal plane compared to edge sites which leads to strong interaction with hydrogen ion, this may be hindrance for the evolution of hydrogen gas. Further, we conducted an analysis of the total and partial electronic

Table 2
Calculated ΔE^{H}_{ads}, ΔG^{H} and Löwdin charge of HER activity over pristine HfS_2, $HfSe_2$ and HfSSe monolayers.

Systems	Adsorption Site	ΔE^{H} (eV)	$\Delta E_{ZPE} - T\Delta S$ (eV)	ΔG^{H} (eV)	Löwdin charge	
					Q_H(e)	ΔQ_H (e)
HfS_2	Hf	1.85	0.30	2.09	1.28	0.28
	S	1.39	0.30	1.69	1.26	0.26
$HfSe_2$	Hf	1.56	0.30	1.86	1.41	0.41
	Se	1.44	0.30	1.74	1.23	0.23
HfSSe	Hf (Se-plane)	1.57	0.37	1.94	1.28	0.28
	Hf (S-plane)	1.85	0.37	2.22	1.34	0.34
	S-edge	1.16	0.37	1.53	1.17	0.17
	Se-edge	1.48	0.37	1.85	1.23	0.23

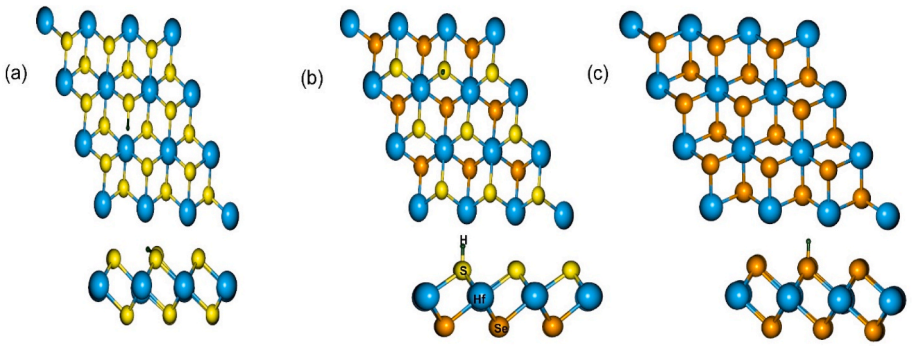

Fig. 3. The optimized geometries of H-adsorbed (a) HfS_2, (b) HfSSe and (c) $HfSe_2$ monolayers.

Table 3
Calculated lattice constant (a), bond lengths, Formation energy, ΔE^{H}_{ads}, ΔG^{H} and ΔQ_H of defected HfS_2, $HfSe_2$ and HfSSe monolayers.

System	a (Å)	Bond length (Å)	E_{form} (eV)	Adsorption site	ΔE^{H} (eV)	$\Delta E_{ZPE} - T\Delta S$ (eV)	ΔG^{H} (eV)	ΔQ_H (eV)
HfS_2-V_{Hf}	10.92	2.58	3.53	Hf	−0.20	0.35	0.15	0.30
HfS_2-V_S	10.93	2.58	6.95	Hollow	−1.21	0.35	−0.86	0.63
$HfSe_2$-V_{Hf}	11.11	2.70	2.96	Hollow	−0.02	0.35	0.33	0.42
$HfSe_2$-V_{Se}	11.15	2.67	5.86	Hf (moved to hollow site)	−1.29	0.35	−0.94	0.70
HfSSe-V_{Hf}	11.03	2.42 (Hf–S) 2.68 (Hf–Se)	5.95	S	0.01	0.33	0.34	0.17
HfSSe-V_S	11.05	2.57 (Hf–S) 2.68 (Hf–Se)	4.52	Hf	−1.23	0.33	−0.90	0.34
HfSSe-V_{Se}	11.03	2.57 (Hf–S) 2.68 (Hf–Se)	2.90	Hollow	−1.19	0.33	−0.86	0.68

density of states (PDOS) for H adsorption on various configurations of HfS_2, Janus HfSSe, and $HfSe_2$. This study aimed to provide deeper insights into the adsorption behaviour of H in different positions. Following the adsorption of H onto these pristine systems, they exhibited metallic properties, confirming a notable interaction between H and the catalyst materials. The concept of DOS is crucial in grasping the physical characteristics of materials, as it offers a straightforward method to depict intricate electronic structures. Essential features that are pivotal in determining the electrical and optical attributes of materials, such as the band gap and the effective masses of charge carriers, are readily observable in the DOS representation [69]. The PDOS analysis revealed that the hydrogen atoms contribution, particularly in the vicinity of the Fermi level, can be attributed to weak interaction towards H. Fig. 4 shows the PDOS of the three systems providing good catalytic efficiency as S-site HfS_2, Se-site $HfSe_2$ and S-edge site HfSSe. In case of pristine HfS_2, the contribution of H atom is more towards the conduction band indicating physisorption, whereas, in case of pristine $HfSe_2$, the contribution of H atom is also more towards the conduction band providing same analysis of physisorption as HfS_2. In case of Janus HfSSe, the contribution of H atom has a small peak near conduction band indicating physisorption. On the other hand, the interaction of hydrogen state with adsorbate states gives rise to bonding and anti-bonding states which can be attributed to lesser interaction with hydrogen atoms and helps to desorb easily. We can conclude from our previous discussion that edge sites of HfS_2 and $HfSe_2$ are more active as compared to basal plane but among the three pristine systems S-edge site of HfSSe provides the best catalytic efficiency for HER. In the past, there was a prevailing notion that the active edge sites of transition metal dichalcogenide (TMD) catalysts posed a significant obstacle to efficient hydrogen production [9,17,70]. As a result, a potential solution to this challenge has been suggested: by enhancing the reactivity of the basal plane, it could help to overcome this issue. One of the most commonly known method to improve the activity of basal plane is by introducing various defects that have previously shown increment in catalytic efficiency [24–27]. Thus, we can consider the possibility of enhancement of catalytic efficiency of HfS_2, $HfSe_2$ and Janus HfSSe by defect creation.

3.4. Structural properties of defected structures

We are interested to investigate the role of defected monolayers towards the HER performance. Therefore, we have created mono transition metal and chalcogenides vacancies namely monohafnium vacancy (V_{Hf}), monosulphur vacancy (V_S) and monoselenium vacancy (V_{Se}) correspondingly. All the different vacancies formed monolayers are depicted in Fig. S1. Defect is a method used to finely adjust the essential electronic characteristics of the material. This serves as a fundamental strategy to elevate the catalytic performance of a catalyst. After thorough optimization of various functionalized systems, we observed that there were minimal alterations in the overall structure. After the creation of defects in HfS_2, $HfSe_2$ and HfSSe structures, we observe decrement in the lattice constants shown in Table 3, attributed to the fact that the ions around these vacancies relax inwardly as observed in various previous studies [71]. We have calculated the formation energy in the chalcogenide rich condition with the formula used in elsewhere [58]. Our results are quite in agreement with the pervious report, the chalcogenides vacancy are quite favourable as they have lower formation energy than transition metal vacancy. The formation energy is listed in the Table 3. Both the vacancies are observed experimentally [58,72], therefore, we have carried out HER activity.

3.5. Electronic properties of defected structure

To assess the improvement in the HER activity of defected systems, we introduced H onto the defect sites shown in Fig. 5. We observe that the favourable position for hydrogen to get absorbed is still sulphur site, which is similar to the case without defects in case of HfS_2 and Janus HfSSe. However, in the case of $HfSe_2$, hydrogen prefers to the hollow site leading to have lower adsorption energy, which is comparable to the Hf-defect in Janus HfSSe. To get insight, on the effect of hydrogen adsorption on the changed catalyst, we investigated the electronic properties of defected HfS_2, $HfSe_2$ and Janus HfSSe before (top panel of Fig. 6) and after hydrogen adsorbed (bellow panel of the Fig. 6). Fig. 6 *depicts* the PDOS of lowest ΔG^{H}.

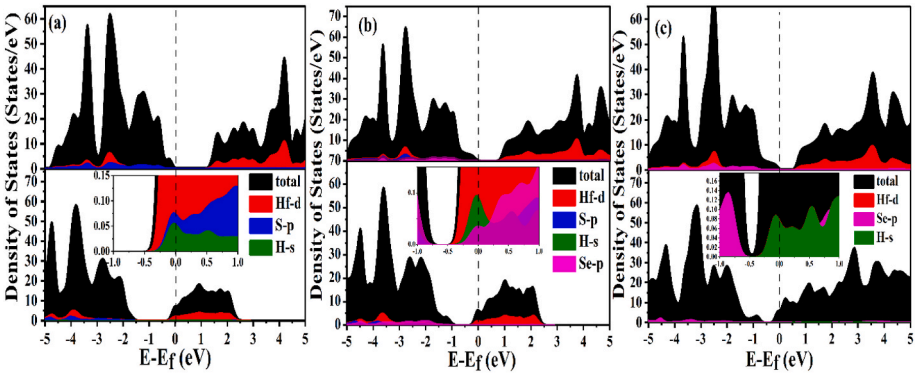

Fig. 4. PDOS for H-adsorption on pristine (a) HfS_2, (b) HfSSe and (c) $HfSe_2$ monolayers.

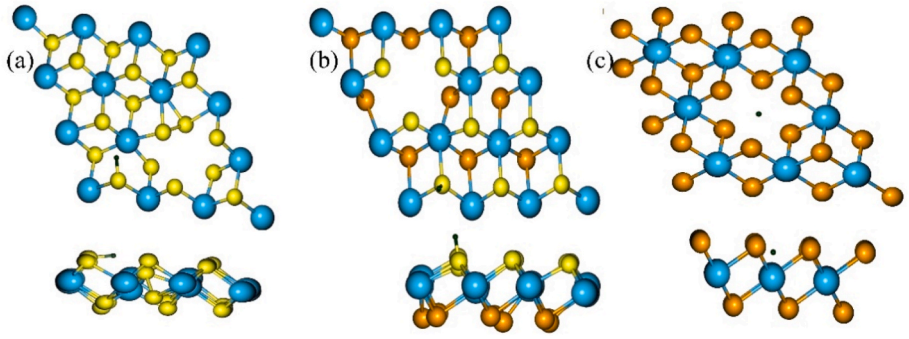

Fig. 5. The optimized structure of various defect engineered (a) HfS_2, (b) HfSSe and (c) $HfSe_2$ monolayers.

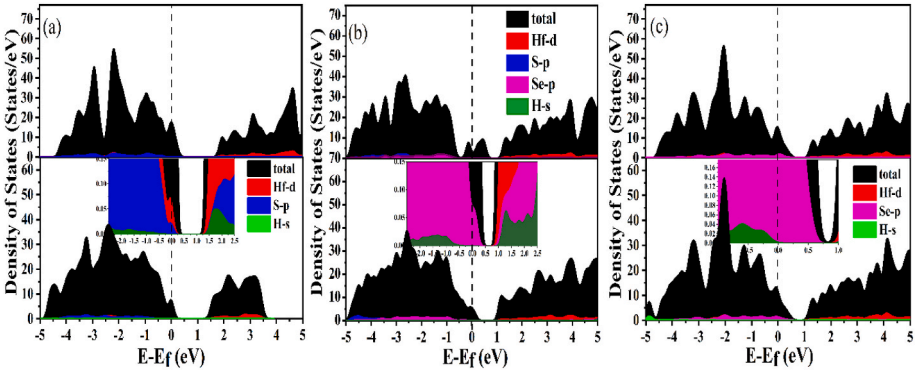

Fig. 6. PDOS of H-adsorption over the defect engineered (a) HfS_2, (b) HfSSe and (c) $HfSe_2$ monolayers.

The defect formation in all cases causes semiconductor-to-metal transition which agrees with previous DFT studies [58,72]. The metallic nature of the mono vacancy TMDs and Janus, have high electrical conductivity, which facilitates efficient charge transfer during electrocatalysis. This conductivity is crucial for the rapid transport of electrons to the active sites on the catalyst surface, promoting a more effective HER. It is observed that all the systems after H-adsorption remains metallic in nature. On the Top panel of Fig. 6, we observed there is decrease in the TDOS near the Fermi level, suggests their involvement in bond formation with the adsorbate. Additionally, we've noted that in case of HfS_2, the PDOS of H exhibits higher density in the conduction band. A similar pattern is observed in the PDOS of $HfSe_2$ in case of V_{Hf} at hollow site and HfSSe as shown in Fig. 6. This phenomenon aligns with the nature of optimal interaction, which is consistent with our findings from ΔG^H calculations. However, when H states interact with adsorbate states, it contributes in both bonding and anti-bonding states.

These states indicate a weaker interaction with H atom, making it easier for them to desorb from the system. Furthermore, using the lowdin charge analysis, we observed the chalcogenide (S or Se) defect leads to higher charge transfer as compared to the Hafnium defect as seen from ***Tabel 3***. This higher charge transfer may be the reason for the interaction which might be a hindrance for the hydrogen evolution reaction. Thereafter, we have compared the ΔG^H of our work with the previously reported TMDs, in the volcano plot (Fig. S2). We found that not only basal activity of Hf-defected HfS_2 increases but falls in the best catalyst shaded region followed by other two defected system $HfSe_2$-V_{Hf}-Hollow site and HfSSe-V_{Hf}-S site. Their ΔG^H is comparable to CoS_2, CrS_2, FeS_2, Co-doped HfS_2, P-doped HfS_2 TMDs [73–81]. ***Table S1*** shows the comparison of ΔG^H of all the stable 2D-TMDs with HfS_2 and $HfSe_2$ monolayers which is shown in the supplementary information.

3.6. Catalytic properties of defected structures

Subsequently, we calculated the ΔE^H_{ads} and determined the ΔG^H for defected monolayers, utilizing equations (3) and (4). We have observed that defect engineering has indeed enhanced the catalytic efficiency as seen from the obtained ΔE^H_{ads} and ΔG^H values denoted in Table 3. Here, we can analyze that in case of HfS_2, V_{Hf} gives us lower ΔG^H as compared to V_S and its parent structure. Further, in case of $HfSe_2$, it is observed that, V_{Hf} gives lower ΔG^H as compared to V_{Se} and its parent structure. Whereas, in case of Janus HfSSe, the order of lowest ΔG^H is for V_{Hf}, followed by V_{Se} and V_S. Also, we can conclude that defected HfS_2 gives us the lowest ΔG^H followed by defected $HfSe_2$ and defected Janus HfSSe with values 0.15 eV, 0.33 eV and 0.34 eV respectively. From the above discussion we can conclude that V_{Hf} in case of HfS_2 is best-suited for HER as its value is closer to zero which is the ideal value. Finally, we conclude that the defected system helps to increase basal plane activity of TMD.

3.7. Comparison of Volmer-Heyrovsky and Volmer-Tafel mechanism

In our effort to boost Hydrogen Evolution Reaction (HER), we looked at two ways in which it can happen: Volmer-Heyrovsky and Volmer-Tafel reactions. For investigating it, we considered the systems having the lowest Volmer-Gibbs free energy. We found that when we added a second proton near the Volmer-Hydrogen (H_{Vol}), about 2 Å away, the Volmer-Heyrovsky reaction was way more effective. On the flip side, putting the second proton on top of the atom close to Volmer-hydrogen in the Volmer-Tafel mechanism didn't work as well. Volmer-Heyrovsky has an upper hand in better HER activity. Out of three pristine monolayers, the Janus exhibit the lowest Gibbs free energy. Therefore, we include the description mechanism of it alongwith the reaction coordinates (see Fig. 7). The calculated Volmer-Heyrovsky Gibbs free energy (ΔG^{HV}) for Janus HfSSe is found to be 0.30 eV and we observed the evolution of hydrogen in the process. To investigate the Volmer-Tafel, we adsorbed the second proton on top of the sulphur ($H_{T\text{-}S}$) and hafnium ($H_{T\text{-}Hf}$) atoms.

The lowest adsorption energy for the second hydrogen is found to be

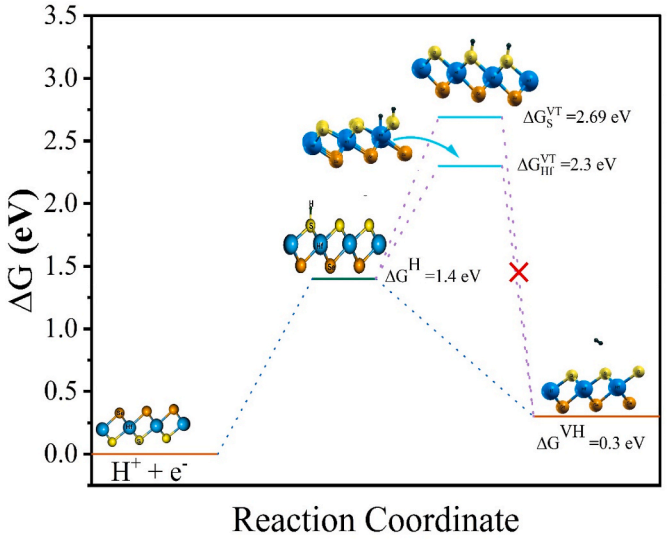

Fig. 7. Reaction coordinate of Jannus HfSSe.

0.07 eV for the hafnium site, whereas in case of S, it is 0.47 eV. It is interesting to note that after the adsorption of second hydrogen, the distance between the H_{Vol} and $H_{T\text{-}Hf}$ and H_{Vol} and $H_{T\text{-}S}$ is 2.23 Å and 2.86 Å respectively. These two adsorbed hydrogens on Janus monolayer are observed to move way from each other rather than interacting. The final distance between H_{Vol} and $H_{T\text{-}Hf}$ and H_{Vol} and $H_{T\text{-}S}$ is found to be 2.5 Å and 3.72 Å respectively. The calculated Volmer-Tafel Gibbs energy (ΔG^{HT}) is found to be 2.30 and 2.69 eV for Hf and S positions respectively. This suggests that the hydrogen evolution reaction is possible with Volmer-Heyrovsky rather than Volmer-Tafel reaction. We conclude that the chalcogenides are a hindrance in the Volmer-Tafel reaction leading to low production of hydrogen. Similar results were obtained for other two pristine monolayers, whose starting and ending setups of pristine monolayers are pictorially represented in SI (Fig. S3 -S5). In the case of HfS_2-Hf defect, we observed the evolution of H_2S. This phenomenon was previously observed in the MoS_2 and MoS_2-sulphur vacancies [82–84]. In this scenario, hydrogen sulphide will cease to desorb in large quantities when the evolution of hydrogen becomes more practical than the desorption of sulphur and the further adsorption of hydrogen. In nutshell, sulphur will continue to desorb as H_2S, until the evolution of hydrogen becomes the more kinetically preferred process. This finding is a big step forward in making hydrogen production more effective. We did not observe the evolution of H_2Se, in case of defected-$HfSe_2$. The sole reason behind the evolution of H_2S in defected HfS_2 is the electronegativity of sulphur which is lower than selenide. Therefore, the evolution of H_2Se is not observed, which promotes only H_2 evolution through VH mechanism. Even in case of Janus-defect, due to presence of selenide layer, it prohibits the evolution of H_2S as compared to HfS_2-def-monolayer (final snapshot provided in SI; Fig. S3).

4. Conclusion

We investigated the structural and electronic properties, along with the catalytic activities, of pristine and defected HfS_2, Janus HfSSe, and $HfSe_2$ monolayers. Our calculations revealed that pristine HfS_2, $HfSe_2$ and HfSSe possesses electronic band gaps in range of infrared-visible, making them suitable candidates for their use as photo-catalysts. The computed ΔE_{ads}^{H} and ΔG^H for H reveals that the Janus structure exhibits higher catalytic activity compared to HfS_2 and $HfSe_2$ monolayer, as was observed in Janus SeMoS. Further, the introduction of mono Hafnium and chalcogenide (S,Se) defects into these materials, had a profound impact on their electronic properties, that revealed semiconductor-to-metal transition. This transition provides higher electrical conductivity, which facilitates efficient charge transfer during electrocatalysis. The presence of a V_{Hf} resulted in a lower ΔG^H compared to the presence of V_S or the pristine structure. Similarly, for $HfSe_2$, V_{Hf} exhibited lower ΔG^H values compared to V_{Se} or the pristine structure. As for Janus HfSSe, V_{Hf} displayed the lowest ΔG^H, followed by V_{Se} and V_S. Our analysis indicated that defected HfS_2 exhibited the most favourable ΔG^H, followed by defected $HfSe_2$ and defected Janus HfSSe, with values of 0.15 eV, 0.33 eV, and 0.334 eV, respectively. Furthermore, a competition is observed between the evolution of H_2S and H_2 gas in the case of HfS_2-V_{Hf}. In contrast, defected Janus and $HfSe_2$, characterized by Se layers, show no competitiveness with H_2S or H_2Se gases. These materials exhibit lower reactional Gibbs free energy compared to the pristine monolayers due to their metallic nature, underscoring their catalytic potential. The research also notes an enhanced hydrogen evolution reaction (HER) activity associated with Hafnium vacancies, with the Volmer-Heyrovsky reaction dominating the catalytic mechanism. These findings contribute valuable insights into the design and optimization of catalysts for efficient HER processes.

CRediT authorship contribution statement

Archana N. Inamdar: Conceptualization, Data curation, Formal analysis, Investigation, Methodology, Validation, Visualization, Writing – original draft, Writing – review & editing. **Narayan N. Som:** Data curation, Formal analysis, Methodology, Visualization, Writing – original draft, Investigation, Validation. **Shweta Dabhi:** Resources, Methodology, Visualization, Writing – review & editing. **Arun Pratap:** Supervision. **Piotr Spiewak:** Resources. **Krzysztof Kurzydłowski:** Resources. **Prafulla K. Jha:** Conceptualization, Supervision, Writing – review & editing.

Declaration of competing interest

The authors declare no competing financial interest. There are no conflicts to declare.

Acknowledgements

This research was carried out with the support of the Interdisciplinary Centre for Mathematical and Computational Modelling (ICM), University of Warsaw, Poland, under Grants no. GB84-17. Part of the calculations were performed on PARAM Shavak HPC installed at CHARUSAT, Gujarat, India. Authors are thankful to DST-FIST (SR/FST/PS-I/2022/230), Government of India, for financial assistance and Polish high-performance computing infrastructure PLGrid (HPC Centers: ACK Cyfronet AGH, PCSS, WCSS) for providing computer facilities and support within computational grant no. PLG/2022/015987.

Appendix A. Supplementary data

Supplementary data to this article can be found online at https://doi.org/10.1016/j.ijhydene.2024.04.143.

References

[1] Novoselov KS, Geim AK, Morozov SV, Jiang D, Katsnelson MI, Grigorieva IV, et al. Two-dimensional gas of massless Dirac fermions in graphene. Nature 2005;438:197–200. https://doi.org/10.1038/nature04233.
[2] Gusynin VP, Sharapov SG. Unconventional integer quantum Hall effect in graphene. Phys Rev Lett 2005;95:146801. https://doi.org/10.1103/PhysRevLett.95.146801.
[3] Dunn B, Kamath H, Tarascon J-M. Electrical energy storage for the grid: a battery of choices. Science 2011;334:928–35. https://doi.org/10.1126/science.1212741. 1979.
[4] Yang Z, Zhang J, Kintner-Meyer MCW, Lu X, Choi D, Lemmon JP, et al. Electrochemical energy storage for green grid. Chem Rev 2011;111:3577–613. https://doi.org/10.1021/cr100290v.

[5] Mohajeri S, Noei M, Salari AA, Hoseini Z, Ahmadaghaei N, Molaei N. Adsorption of phosphine on a BN nanosurface. Iran. J Chem Chem Eng 2018;37(1):39–45. https://doi.org/10.30492/IJCCE.2018.26372.

[6] Nazari Kudahi S, Noorpoor A, Mahmoodi NM. Adsorption performance indicator for power plant CO_2 capture on graphene oxide/TiO_2 nanocomposite. Iran. J Chem Chem Eng 2019;38(3):293–307. https://doi.org/10.30492/IJCCE.2019.31728.

[7] Seh ZW, Kibsgaard J, Dickens CF, Chorkendorff I, Nørskov JK, Jaramillo TF. Combining theory and experiment in electrocatalysis: insights into materials design. Science 2017:355. https://doi.org/10.1126/science.aad4998. 1979.

[8] Wang J, Gao Y, Kong H, Kim J, Choi S, Ciucci F, et al. Non-precious-metal catalysts for alkaline water electrolysis: *operando* characterizations, theoretical calculations, and recent advances. Chem Soc Rev 2020;49:9154–96. https://doi.org/10.1039/D0CS00575D.

[9] Eftekhari A. Electrocatalysts for hydrogen evolution reaction. Int J Hydrogen Energy 2017;42:11053–77. https://doi.org/10.1016/j.ijhydene.2017.02.125.

[10] Li R, Li C. Photocatalytic water splitting on semiconductor-based photocatalysts. 1–57, https://doi.org/10.1016/bs.acat.2017.09.001; 2017.

[11] Di J, Yan C, Handoko AD, Seh ZW, Li H, Liu Z. Ultrathin two-dimensional materials for photo- and electrocatalytic hydrogen evolution. Mater Today 2018;21:749–70. https://doi.org/10.1016/j.mattod.2018.01.034.

[12] Alizadeh M, Tong GB, Mehmood MS, Qader KW, Rahman SA, Shokri B. Band engineered Al-rich InAlN thin films as a promising photoanode for hydrogen generation from solar water splitting. Sol Energy Mater Sol Cell 2018;185:445–55. https://doi.org/10.1016/j.solmat.2018.05.058.

[13] Roger I, Shipman MA, Symes MD. Earth-abundant catalysts for electrochemical and photoelectrochemical water splitting. Nat Rev Chem 2017;1:3. https://doi.org/10.1038/s41570-016-0003.

[14] Inamdar AN, Som NN, Pratap A, Jha PK. Hydrogen evolution and oxygen evolution reactions of pristine and alkali metal doped $SnSe_2$ monolayer. Int J Hydrogen Energy 2020;45:18657–65. https://doi.org/10.1016/j.ijhydene.2019.07.093.

[15] Kibsgaard J, Chorkendorff I. Considerations for the scaling-up of water splitting catalysts. Nat Energy 2019;4:430–3. https://doi.org/10.1038/s41560-019-0407-1.

[16] Faber MS, Jin S. Earth-abundant inorganic electrocatalysts and their nanostructures for energy conversion applications. Energy Environ Sci 2014;7:3519–42. https://doi.org/10.1039/C4EE01760A.

[17] Zou X, Zhang Y. Noble metal-free hydrogen evolution catalysts for water splitting. Chem Soc Rev 2015;44:5148–80. https://doi.org/10.1039/C4CS00448E.

[18] Chhowalla M, Shin HS, Eda G, Li L-J, Loh KP, Zhang H. The chemistry of two-dimensional layered transition metal dichalcogenide nanosheets. Nat Chem 2013;5:263–75. https://doi.org/10.1038/nchem.1589.

[19] Merki D, Vrubel H, Rovelli L, Fierro S, Hu X. Fe, Co, and Ni ions promote the catalytic activity of amorphous molybdenum sulfide films for hydrogen evolution. Chem Sci 2012;3:2515. https://doi.org/10.1039/c2sc20539d.

[20] Benck JD, Hellstern TR, Kibsgaard J, Chakthranont P, Jaramillo TF. Catalyzing the hydrogen evolution reaction (HER) with molybdenum sulfide nanomaterials. ACS Catal 2014;4:3957–71. https://doi.org/10.1021/cs500923c.

[21] Ding Y, Wang Y, Ni J, Shi L, Shi S, Tang W. First principles study of structural, vibrational and electronic properties of graphene-like MX_2 (M=Mo, Nb, W, Ta; X=S, Se, Te) monolayers. Phys B Condens Matter 2011;406:2254–60. https://doi.org/10.1016/j.physb.2011.03.044.

[22] Yi Y, Chen Z, Yu X, Zhou Z, Li J. Recent advances in quantum effects of 2D materials. Adv Quantum Technol 2019;2. https://doi.org/10.1002/qute.201800111.

[23] El-Emam RS, Özcan H. Comprehensive review on the techno-economics of sustainable large-scale clean hydrogen production. J Clean Prod 2019;220:593–609. https://doi.org/10.1016/j.jclepro.2019.01.309.

[24] Zhang W, Zhou K. Ultrathin two-dimensional nanostructured materials for highly efficient water oxidation. Small 2017;13:1700806. https://doi.org/10.1002/smll.201700806.

[25] Jin H, Guo C, Liu X, Liu J, Vasileff A, Jiao Y, et al. Emerging two-dimensional nanomaterials for electrocatalysis. Chem Rev 2018;118:6337–408. https://doi.org/10.1021/acs.chemrev.7b00689.

[26] Chen Y, Yang K, Jiang B, Li J, Zeng M, Fu L. Emerging two-dimensional nanomaterials for electrochemical hydrogen evolution. J Mater Chem A Mater 2017;5:8187–208. https://doi.org/10.1039/C7TA00816C.

[27] Jia Y, Chen J, Yao X. Defect electrocatalytic mechanism: concept, topological structure and perspective. Mater Chem Front 2018;2:1250–68. https://doi.org/10.1039/C8QM00070K.

[28] Tang C, Zhang Q. Nanocarbon for oxygen reduction electrocatalysis: dopants, edges, and defects. Adv Mater 2017;29:1604103. https://doi.org/10.1002/adma.201604103.

[29] Toh RJ, Sofer Z, Pumera M. Catalytic properties of group 4 transition metal dichalcogenides (MX_2 ; M = Ti, Zr, Hf; X = S, Se, Te). J Mater Chem A Mater 2016;4:18322–34. https://doi.org/10.1039/C6TA08089H.

[30] Cui H, Jia P, Peng X. Adsorption of SO_2 and NO_2 molecule on intrinsic and Pd-doped HfSe2 monolayer: a first-principles study. Appl Surf Sci 2020;513:145863. https://doi.org/10.1016/j.apsusc.2020.145863.

[31] Song H-Y, Sun J-J, Li M. Enhancement of monolayer $HfSe_2$ thermoelectric performance by strain engineering: a DFT calculation. Chem Phys Lett 2021;784:139109. https://doi.org/10.1016/j.cplett.2021.139109.

[32] Obodo KO, Gebreyesus G, Ouma CNM, Obodo JT, Ezeonu SO, Rai DP, et al. Controlling the electronic and optical properties of HfS_2 mono-layers *via* lanthanide substitutional doping: a DFT+*U* study. RSC Adv 2020;10:15670–6. https://doi.org/10.1039/D0RA02464C.

[33] Faghihnasiri M, Ahmadi A, Alvankar Golpayegan S, Garosi Sharifabadi S, Ramazani A. A first-principles study of nonlinear elastic behavior and anisotropic electronic properties of two-dimensional HfS_2. Nanomaterials 2020;10:446. https://doi.org/10.3390/nano10030446.

[34] Salavati M. Electronic and mechanical responses of two-dimensional HfS_2, $HfSe_2$, ZrS_2, and $ZrSe_2$ from first-principles. Front Struct Civ Eng 2019;13:486–94. https://doi.org/10.1007/s11709-018-0491-5.

[35] Barhoumi M, Lazaar K, Bouzidi S, Said M. A DFT study of Janus structure of S and Se in HfSSe layered as a promising candidate for electronic devices. J Mol Graph Model 2020;96:107511. https://doi.org/10.1016/j.jmgm.2019.107511.

[36] Hu J, Zhang Q, Zhang Q, Cui H. Favorable sensing property of Pt-doped Janus HfSSe monolayer upon H_2S and SO_2: a first-principles theory. J Mater Res Technol 2022;20:763–71. https://doi.org/10.1016/j.jmrt.2022.07.080.

[37] Hoat DM, Naseri M, Hieu NN, Ponce-Pérez R, Rivas-Silva JF, Vu TV, et al. A comprehensive investigation on electronic structure, optical and thermoelectric properties of the HfSSe Janus monolayer. J Phys Chem Solid 2020;144:109490. https://doi.org/10.1016/j.jpcs.2020.109490.

[38] Greenaway DL, Nitsche R. Preparation and optical properties of group IV–VI chalcogenides having the CdI_2 structure. J Phys Chem Solid 1965;26:1445–58. https://doi.org/10.1016/0022-3697(65)90043-0.

[39] Moustafa M, Zandt T, Janowitz C, Manzke R. Growth and band gap determination of the ZrS_xSe_{2-x} single crystal series. Phys Rev B 2009;80:035206. https://doi.org/10.1103/PhysRevB.80.035206.

[40] Jiang H. Structural and electronic properties of ZrX_2 and HfX_2 (X = S and Se) from first principles calculations. J Chem Phys 2011;134. https://doi.org/10.1063/1.3594205.

[41] Yan D, Li Y, Huo J, Chen R, Dai L, Wang S. Defect chemistry of nonprecious-metal electrocatalysts for oxygen reactions. Adv Mater 2017;29:1606459. https://doi.org/10.1002/adma.201606459.

[42] Lou H, Yu G, Tang M, Chen W, Yang G. Janus MoPC monolayer with superior electrocatalytic performance for the hydrogen evolution reaction. ACS Appl Mater Interfaces 2022;14:7836–44. https://doi.org/10.1021/acsami.1c20114.

[43] Wang D, Zhang X, Wang Z. Recent advances in properties, synthesis and applications of two-dimensional HfS_2. J Nanosci Nanotechnol 2018;18:7319–34. https://doi.org/10.1166/jnn.2018.16042.

[44] Yao Q, Zhang L, Bampoulis P, Zandvliet HJW. Nanoscale investigation of defects and oxidation of $HfSe_2$. J Phys Chem C 2018;122:25498–505. https://doi.org/10.1021/acs.jpcc.8b08713.

[45] Singh D, Chakraborty S, Ahuja R. Emergence of Si_2BN monolayer as efficient HER catalyst under Co-functionalization influence. ACS Appl Energy Mater 2019;2:8441–8. https://doi.org/10.1021/acsaem.9b01292.

[46] Giannozzi P, Baroni S, Bonini N, Calandra M, Car R, Cavazzoni C, et al. QUANTUM ESPRESSO: a modular and open-source software project for quantum simulations of materials. J Phys Condens Matter 2009;21:395502. https://doi.org/10.1088/0953-8984/21/39/395502.

[47] Perdew JP, Burke K, Wang Y. Generalized gradient approximation for the exchange-correlation hole of a many-electron system. Phys Rev B 1996;54:16533–9. https://doi.org/10.1103/PhysRevB.54.16533.

[48] Grimme S. Semiempirical GGA-type density functional constructed with a long-range dispersion correction. J Comput Chem 2006;27:1787–99. https://doi.org/10.1002/jcc.20495.

[49] Pack JD, Monkhorst HJ. "Special points for Brillouin-zone integrations"—a reply. Phys Rev B 1977;16:1748–9. https://doi.org/10.1103/PhysRevB.16.1748.

[50] Almeida R, Banerjee A, Chakraborty S, Almeida J, Ahuja R. Theoretical evidence behind bifunctional catalytic activity in pristine and functionalized Al_2C monolayers. ChemPhysChem 2018;19:148–52. https://doi.org/10.1002/cphc.201700768.

[51] Chodvadiya D, Som NN, Jha PK, Chakraborty B. Enhancement in the catalytic activity of two-dimensional α-CN by B, Si and P doping for hydrogen evolution and oxygen evolution reactions. Int J Hydrogen Energy 2021;46:22478–98. https://doi.org/10.1016/j.ijhydene.2021.04.080.

[52] Lee CH, Jun B, Lee SU. Theoretical evaluation of the structure–activity relationship in graphene-based electrocatalysts for hydrogen evolution reactions. RSC Adv 2017;7:27033–9. https://doi.org/10.1039/C7RA04115B.

[53] Bera J, Betal A, Sahu S. Spin orbit coupling induced enhancement of thermoelectric performance of HfX_2 (X = S, Se) and its Janus monolayer. J Alloys Compd 2021;872:159704. https://doi.org/10.1016/j.jallcom.2021.159704.

[54] Huynh TMD, Nguyen DK, Nguyen TDH, Dien VK, Pham HD, Lin M-F. Geometric and electronic properties of monolayer HfX_2 (X = S, Se, or Te): a first-principles calculation. Front Mater 2021;7. https://doi.org/10.3389/fmats.2020.569756.

[55] Dabral A, Lu AKA, Chiappe D, Houssa M, Pourtois G. A systematic study of various 2D materials in the light of defect formation and oxidation. Phys Chem Chem Phys 2019;21:1089–99. https://doi.org/10.1039/C8CP05665J.

[56] Kumar P, Sharma V, Shirodkar SN, Dev P. Predicting phase preferences of two-dimensional transition metal dichalcogenides using machine learning. Phys Rev Mater 2022;6:094007. https://doi.org/10.1103/PhysRevMaterials.6.094007.

[57] Zhao Q, Guo Y, Si K, Ren Z, Bai J, Xu X. Elastic, electronic, and dielectric properties of bulk and monolayer ZrS_2 , $ZrSe_2$, HfS_2 , $HfSe_2$ from van der Waals density-functional theory. Phys Status Solidi 2017;254. https://doi.org/10.1002/pssb.201700033.

[58] Zhao X, Gao Y, Zhang H, Wang H, Wang T, Wei S. Effect of structural defects and S-doped on electronic structure and magnetic properties of $HfSe_2$ monolayer. J Magn Magn Mater 2019;479:192–8. https://doi.org/10.1016/j.jmmm.2019.02.029.

[59] Laursen AB, Varela AS, Dionigi F, Fanchiu H, Miller C, Trinhammer OL, et al. Electrochemical hydrogen evolution: sabatier's principle and the volcano plot. J Chem Educ 2012;89:1595–9. https://doi.org/10.1021/ed200818t.

[60] Mir SH, Chakraborty S, Wärnå J, Narayan S, Jha PC, Jha PK, et al. A comparative study of hydrogen evolution reaction on pseudo-monolayer WS_2 and PtS_2 : insights

based on the density functional theory. Catal Sci Technol 2017;7:687–92. https://doi.org/10.1039/C6CY02426B.
[61] Fang Y-H, Wei G-F, Liu Z-P. Catalytic role of minority species and minority sites for electrochemical hydrogen evolution on metals: surface charging, coverage, and Tafel kinetics. J Phys Chem C 2013;117:7669–80. https://doi.org/10.1021/jp400608p.
[62] Di J, Yan C, Handoko AD, Seh ZW, Li H, Liu Z. Ultrathin two-dimensional materials for photo- and electrocatalytic hydrogen evolution. Mater Today 2018;21:749–70. https://doi.org/10.1016/j.mattod.2018.01.034.
[63] Eftekhari A, Fang B. Electrochemical hydrogen storage: opportunities for fuel storage, batteries, fuel cells, and supercapacitors. Int J Hydrogen Energy 2017;42:25143–65. https://doi.org/10.1016/j.ijhydene.2017.08.103.
[64] Qian Z, Jiao L, Xie L. Phase engineering of <scp>Two-Dimensional</scp> transition metal dichalcogenides. Chin J Chem 2020;38:753–60. https://doi.org/10.1002/cjoc.202000064.
[65] Kibsgaard J, Chen Z, Reinecke BN, Jaramillo TF. Engineering the surface structure of MoS2 to preferentially expose active edge sites for electrocatalysis. Nat Mater 2012;11:963–9. https://doi.org/10.1038/nmat3439.
[66] Lukowski MA, Daniel AS, Meng F, Forticaux A, Li L, Jin S. Enhanced hydrogen evolution catalysis from chemically exfoliated metallic MoS_2 nanosheets. J Am Chem Soc 2013;135:10274–7. https://doi.org/10.1021/ja404523s.
[67] Lee J, Kang S, Yim K, Kim KY, Jang HW, Kang Y, et al. Hydrogen evolution reaction at anion vacancy of two-dimensional transition-metal dichalcogenides: ab initio computational screening. J Phys Chem Lett 2018;9:2049–55. https://doi.org/10.1021/acs.jpclett.8b00712.
[68] Zhang J, Jia S, Kholmanov I, Dong L, Er D, Chen W, et al. Janus monolayer transition-metal dichalcogenides. ACS Nano 2017;11:8192–8. https://doi.org/10.1021/acsnano.7b03186.
[69] Toriyama MY, Ganose AM, Dylla M, Anand S, Park J, Brod MK, et al. How to analyse a density of states. Materials Today Electronics 2022;1:100002. https://doi.org/10.1016/j.mtelec.2022.100002.
[70] Teasdale A. Regulatory highlights. Org Process Res Dev 2016;20:1850–4. https://doi.org/10.1021/acs.oprd.6b00355.
[71] Gao X-Y, Zhang J-M, Ali A, Wei X-M, Huang Y-H. Effects of the vacancy and doping on the electronic and magnetic characteristics of $ZrSe_2$ monolayer: a first-principles investigation. Thin Solid Films 2021;732:138790. https://doi.org/10.1016/j.tsf.2021.138790.
[72] Yadav A, Kumar S, Muruganathan M, Kumar R. Defect induced magnetism in monolayer $HfSe_2$: an ab initio study. Appl Surf Sci 2019;491:517–25. https://doi.org/10.1016/j.apsusc.2019.06.119.
[73] Ran N, Sun B, Qiu W, Song E, Chen T, Liu J. Identifying metallic transition-metal dichalcogenides for hydrogen evolution through multilevel high-throughput calculations and machine learning. J Phys Chem Lett 2021;12:2102–11. https://doi.org/10.1021/acs.jpclett.0c03839.
[74] Kc S, Longo RC, Addou R, Wallace RM, Cho K. Impact of intrinsic atomic defects on the electronic structure of MoS_2 monolayers. Nanotechnology 2014;25:375703. https://doi.org/10.1088/0957-4484/25/37/375703.
[75] Pandey M, Rasmussen FA, Kuhar K, Olsen T, Jacobsen KW, Thygesen KS. Defect-tolerant monolayer transition metal dichalcogenides. Nano Lett 2016;16:2234–9. https://doi.org/10.1021/acs.nanolett.5b04513.
[76] Liu G, Peng J, Jia B, Hao J, Zhao Z, Ma X, et al. Catalytic activity for hydrogen evolution reaction of Janus monolayer MoXTe (X=S, Se). Int J Hydrogen Energy 2023;48:13902–12. https://doi.org/10.1016/j.ijhydene.2022.12.306.
[77] Jia B, Peng J, Zhao H, Gao J, Zhao J, Hao J, et al. Defect engineered Janus MoXTe (X=S, Se) monolayers for hydrogen evolution reaction: a first principles study. Int J Hydrogen Energy 2024;51:897–906. https://doi.org/10.1016/j.ijhydene.2023.09.038.
[78] Zhai S, Jiang X, Wu D, Chen L, Su Y, Cui H, et al. Single Rh atom decorated pristine and S-defected PdS2 monolayer for sensing thermal runaway gases in a lithium-ion battery: a first-principles study. Surface Interfac 2023;37:102735. https://doi.org/10.1016/j.surfin.2023.102735.
[79] Wu H, Xia Y, Zhang C, Xie S, Wu S, Cui H. Adsorptions of $C_5F_{10}O$ decomposed compounds on the Cu-decorated NiS_2 monolayer: a first-principles theory. Mol Phys 2023;121. https://doi.org/10.1080/00268976.2022.2163715.
[80] Cui H, Jia P, Peng X. Adsorption of SO2 and NO2 molecule on intrinsic and Pd-doped HfSe2 monolayer: a first-principles study. Appl Surf Sci 2020;513:145863. https://doi.org/10.1016/j.apsusc.2020.145863.
[81] Cui H, Yan C, Jia P, Cao W. Adsorption and sensing behaviors of SF6 decomposed species on Ni-doped C3N monolayer: a first-principles study. Appl Surf Sci 2020;512:145759. https://doi.org/10.1016/j.apsusc.2020.145759.
[82] Abidi N, Bonduelle-Skrzypczak A, Steinmann SN. How stable are 2H-MoS_2 edges under hydrogen evolution reaction conditions? J Phys Chem C 2021;125:17058–67. https://doi.org/10.1021/acs.jpcc.1c04492.
[83] Li G, Zhang D, Qiao Q, Yu Y, Peterson D, Zafar A, et al. All the catalytic active sites of MoS_2 for hydrogen evolution. J Am Chem Soc 2016;138:16632–8. https://doi.org/10.1021/jacs.6b05940.
[84] Tsai C, Abild-Pedersen F, Nørskov JK. Tuning the MoS_2 edge-site activity for hydrogen evolution via support interactions. Nano Lett 2014;14:1381–7. https://doi.org/10.1021/nl404444k.